

Opacities for stellar envelopes

M. J. Seaton,¹ Yu Yan,²* D. Mihalas² and Anil K. Pradhan³

¹Department of Physics and Astronomy, University College London, Gower Street, London WC1E 6BT

²Department of Astronomy, University of Illinois, 1002 W. Green Street, Urbana, IL 61801, USA

³Department of Astronomy, Ohio State University, 174 W. 18th Avenue, Columbus, OH 43210-1106, USA

Accepted 1993 August 27. Received 1993 August 27; in original form 1993 May 4

ABSTRACT

We define stellar envelopes to be those regions of stellar interiors in which atoms exist and are not markedly perturbed by the plasma environment. Availability of accurate and extensive atomic data is a prime requirement for the calculation of envelope opacities. For envelopes we adopt the criterion of mass density $\rho \leq 0.01 \text{ g cm}^{-3}$.

We present radiative Rosseland mean opacities for envelopes obtained using atomic data calculated in an international collaboration referred to as the Opacity Project, or OP. Equations of state are calculated using an occupation-probability formalism. To a good approximation, ionization equilibria and level populations in envelopes depend only on the temperature T and electron density N_e and are insensitive to chemical mixtures. Monochromatic opacities for all abundant chemical elements are therefore calculated on a grid of (T, N_e) values and are archived. Rosseland mean opacities are then readily calculated for any chemical mixture. Tables of Rosseland means, for any required mixtures and as functions of ρ and T , are available on request in computer-readable form.

The present, OP, results are compared with those from another recent study, referred to as OPAL, by C. A. Iglesias and F. A. Rogers at the Lawrence Livermore National Laboratory. The agreement between the OP and OPAL calculations is generally good, although there are some differences. Both calculations give results larger than those obtained in earlier work, by factors of up to 3 or more.

Key words: atomic processes – radiative transfer – stars: interiors.

1 INTRODUCTION

1.1 Basic definitions

Let $I_\nu(s, \hat{n})$ be the intensity of radiation at frequency ν in a direction \hat{n} as a function of distance s . The equation of radiative transfer is

$$dI_\nu/ds = -\kappa_\nu I_\nu + j_\nu, \quad (1)$$

where κ_ν is the opacity and j_ν the emissivity. For a blackbody enclosure at temperature T , I_ν is equal to the Planck function

$$B_\nu(T) = (2h\nu^3/c^2)[\exp(h\nu/kT) - 1]^{-1}, \quad (2)$$

and, since $dI_\nu/ds = 0$,

$$j_\nu/\kappa_\nu = B_\nu(T), \quad (3)$$

which is Kirchhoff's law. Inside a star, conditions are very close to those for a blackbody enclosure, and equation (3)

can certainly be used. The radiation is not, however, completely isotropic since there is a net outwards radiative flux. Using $I_\nu(r, \theta)$ for the intensity at a distance r from the stellar centre and making an angle θ to the direction \hat{r} , the net flux is

$$F_\nu(r) = 2\pi \int_{-1}^{+1} I_\nu(r, \theta) \cos(\theta) d \cos(\theta). \quad (4)$$

Equation (1) may be solved in a diffusion approximation (see Mihalas 1978), assuming small anisotropy, to obtain

$$F_\nu(r) = -\frac{4\pi}{3} \frac{1}{\kappa_\nu} \frac{dB_\nu}{dT} \frac{dT}{dr}. \quad (5)$$

The flux integrated over all frequencies,

$$F(r) = \int_0^\infty F_\nu(r) d\nu, \quad (6)$$

*Present address: Department of Radiation Oncology, Thomas Jefferson University, 111 South 11th Street, Philadelphia PA 19107, USA.

is given by

$$F(r) = -\frac{4\pi}{3} \frac{1}{\kappa_R} \frac{dB(T)}{dT} \frac{dT}{dr}, \quad (7)$$

where

$$B(T) = \int B_\nu(T) d\nu = \frac{2\pi^4 (kT)^4}{15c^2 h^3} \quad (8)$$

and where the *Rosseland mean opacity*, κ_R , is defined by

$$\frac{1}{\kappa_R} \frac{dB(T)}{dT} = \int \frac{1}{\kappa_\nu} \frac{dB_\nu}{dT} d\nu. \quad (9)$$

In the above equations κ_ν is the total opacity for extinction, that is to say including the processes of absorption and scattering. The *Planck mean*, κ_p , is defined by

$$\kappa_p B(T) = \int \tilde{\kappa}_\nu B_\nu d\nu, \quad (10)$$

where $\tilde{\kappa}_\nu$ is the opacity for absorption processes only.

We introduce the variable

$$u = \frac{h\nu}{kT}. \quad (11)$$

Convenient working formulae are

$$\frac{1}{\kappa_R} = \int \frac{1}{\kappa(u)} f_R(u) du, \quad (12)$$

$$\kappa_p = \int \tilde{\kappa}(u) f_p(u) du, \quad (13)$$

where

$$f_R(u) = \frac{15}{4\pi^4} u^4 \exp(-u) [1 - \exp(-u)]^{-2} \quad (14)$$

and

$$f_p(u) = \frac{15}{\pi^5} u^3 \exp(-u) [1 - \exp(-u)]^{-1}. \quad (15)$$

The calculation of Planck means is straightforward in that they do not depend on line profiles (so long as B_ν does not vary significantly over the profiles), and κ_p for a mixture is a simple linear combination of the contributions from the constituents. Calculations of κ_R , a weighted harmonic mean, are more difficult. Information about line profiles is required (a delta-function line gives a zero contribution to κ_R). There is no simple expression giving κ_R for a mixture – the integral in (9) or (12) must be evaluated separately for each mix. Particular attention must be paid to regions in which $\kappa(u)$ is small since such regions can give large contributions to the integrals.

In this section, and throughout this paper, we give all formulae for opacities per unit length. In giving numerical results, however, we follow the usual practice of giving opacities per unit mass (in units of $\text{cm}^2 \text{g}^{-1}$). The relation is

$\kappa(\text{per unit length}) = \rho \times \kappa(\text{per unit mass})$, where ρ is the mass density.

The monochromatic opacity is given by

$$\kappa(u) = \sum_i N_i \{ \sigma_i^{(\text{abs})}(u) [1 - \exp(-u)] + \sigma_i^{(\text{scatt})}(u) \}, \quad (16)$$

where N_i is the number density of particles of type i , $\sigma_i^{(\text{abs})}$ and $\sigma_i^{(\text{scatt})}$ are cross-sections for absorption and scattering processes, and $[1 - \exp(-u)]$ is a correction factor for stimulated emission. Three steps are involved in making opacity calculations: (i) determination of the level populations N_i (the problem of the equation of state); (ii) determination of the atomic cross-sections σ_i ; and (iii) calculation of mean opacities for all required values of temperature, density and chemical composition.

1.2 Previous opacity calculations

Over the years there have been many discussions of discrepancies between ‘astrophysical opacities’ (those adjusted so as to give the best agreement between observations and astrophysical theory) and ‘physical opacities’ (best estimates from physical theory). Such discrepancies were discussed by Eddington (1926), who considered them to be one of the two clouds obscuring theories of stellar structure.¹ The other cloud, concerning the nature of stellar energy sources, was dispersed long ago in consequence of fundamental new discoveries in physics. The fundamental physics required to disperse the opacity cloud has all been known for a long time. The difficulty has been in coping with the sheer complexity of the problem.

In his book ‘The Structure and Evolution of the Stars’, Schwarzschild (1958) considered the determination of opacities to be ‘by far the most bothersome factor in the entire theory’. He took account of just three processes contributing to opacities: bound-free transitions (photoionization), free-free transitions (inverse bremsstrahlung) and electron scattering. Subsequent work has shown that a fourth process, bound-bound transitions (spectrum lines), can make major contributions. That process was first discussed in some detail by Mayer (1948) at the Los Alamos National Laboratory, and some early calculations including lines were made by Moszkowski & Meyerott (1951) and Meyerott & Moszkowski (1951) at the Argonne National Laboratory. During the past 30 years very extensive opacity calculations have been made at Los Alamos [see Cox & Stewart (1962) and Cox (1965) for discussions of the earlier work and Hübner (1985) and Weiss, Keady & Magee (1990) for references to later work]. Results have been made available through the Los Alamos Opacity Library (Hübner et al. 1977), which we refer to as LAOL. Extensive calculations have also been made at St Andrews in Scotland (see Carson, Mayers & Stibbs 1968; Carson 1976).

Despite all of these advances, discussion of discrepancies between ‘physical’ and ‘astrophysical’ opacities has

¹Eddington said that he was recalling a classic phrase of Kelvin. He probably had in mind a lecture which Kelvin gave at the Royal Institution on 1900 April 27, in which reference was made to two clouds obscuring the dynamical theory of heat and light. We are indebted to Dr D. W. Dewhurst for this information.

continued, with particular reference to work on pulsating stars (Fricke, Stobbie & Strittmatter 1971; Petersen 1974; Stellingwerf 1978; Simon 1982; Becker 1985; Andreassen 1989). Simon's (1982) paper was entitled 'A Plea for Re-examining Heavy Element Opacities in Stars'. He showed that several problems in the theory of pulsating stars would be resolved if envelope opacities 2 to 3 times larger than those from LAOL were used. There were two responses to this plea, both taking advantage of advances in computational plasma physics and atomic physics and of the availability of powerful computers. One was work at the Lawrence Livermore National Laboratory (Iglesias, Rogers & Wilson 1987, 1990, 1992; Iglesias & Rogers 1991a,b; Rogers & Iglesias 1992), which is referred to as OPAL, the name of the computer code used. The other was the international Opacity Project, which we refer to as OP and which is the subject of the present paper.

The OPAL paper by Iglesias et al. (1990) was the first to give, for a Cepheid model, opacities enhanced by amounts at least as large as those postulated by Simon (1982).

1.3 Stellar interiors

In stellar interiors both temperatures and densities decrease outwards. In discussing the problems that arise in calculating opacities, it is convenient to regard interiors as being divided into two regions.

(1) *Deep interiors* are regions of high T and ρ . In calculating opacities for these regions the main problem is to allow correctly for plasma correlation effects. In so far as bound states of atomic ions exist at all in deep interiors, they exist only for fairly simple states of highly ionized atoms (such as hydrogenic and He-like). Such states may be highly perturbed by the plasma environment. In deep interiors, conductive opacity may also be important.

(2) *Stellar envelopes* are outer regions with lower values of T and ρ , and are of particular importance for giant stars and for studies of stellar pulsations. In envelopes, complex atomic ions, containing many electrons, exist and can make important contributions to opacities. Such states are not markedly perturbed. For envelopes a main requirement is accurate and very extensive data for free atoms.

Whereas the OPAL work is concerned both with deep interiors and with envelopes, the OP work is concerned only with envelopes. The two approaches may be compared as follows. If, as in the OPAL work, one allows for plasma effects in calculating atomic radiative properties, then one has to use comparatively simple atomic models. The procedure in OPAL is to use central potentials which are adjusted empirically so as to give accurate values for atomic energy levels, and which can be modified so as to allow for plasma effects. The atomic data may then depend on the plasma conditions of temperature and density. In the OPAL work all atomic data are calculated on-line as required, and are not archived. By contrast, the OP work is restricted to envelope regions for which the effects of plasma perturbations on optical properties are not of much importance. All atomic data are calculated once only for unperturbed free atoms, using fairly sophisticated methods which will be described in Section 4. Thus in the envelope regions the OP atomic data should be more accurate than the OPAL data, but this advantage is gained at

the expense of restricting the range of densities for which the OP calculations are valid. An incidental advantage of the OP approach is that we obtain an extensive archive of accurate atomic data which may be of value for various other investigations.

For the presentation of results it is convenient to use the variable

$$R = \rho / T_6^3 \quad (17)$$

introduced in the OPAL work; ρ is the mass density in g cm^{-3} and T_6 the temperature in 10^6 K. Figs 1 and 2 show values of $\log(R)$ against $\log(T)$ for various stars, using data from stellar models provided by Dr Achim Weiss of the Max-Planck-Institut für Astrophysik, Garching (private communication). Fig. 1 shows results for stars on the initial main sequence with masses 1, 2.5, 10 and $50 M_\odot$. The outer part of the $1-M_\odot$ star is convective (shown by a long-dashed line in Fig. 1). In that region the temperature gradient is given by

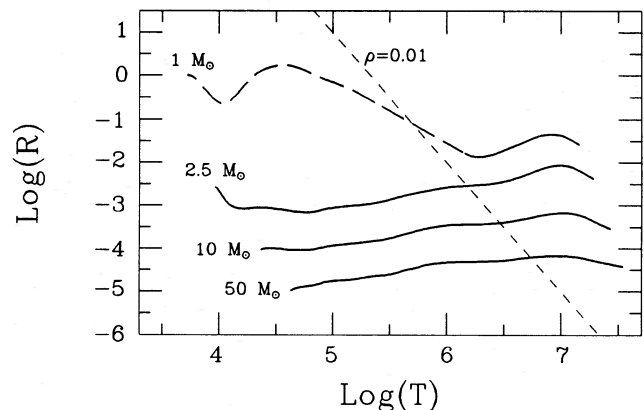


Figure 1. Plots of $\log(R)$ against $\log(T)$ for stars on the initial main sequence. The quantity R is defined by equation (17). Details for the models are $M = 1 M_\odot$, $\log(L/L_\odot) = -0.1057$, $\log(T_{\text{eff}}) = 3.7342$; $M = 2.5 M_\odot$, $\log(L/L_\odot) = 1.5081$, $\log(T_{\text{eff}}) = 3.9821$; $M = 10 M_\odot$, $\log(L/L_\odot) = 3.7394$, $\log(T_{\text{eff}}) = 4.3695$; and $M = 50 M_\odot$, $\log(L/L_\odot) = 5.5597$, $\log(T_{\text{eff}}) = 4.6354$. Compositions are $X = 0.64$, $Z = 0.04$ for the $1-M_\odot$ model and $X = 0.70$, $Z = 0.02$ for the other three models.

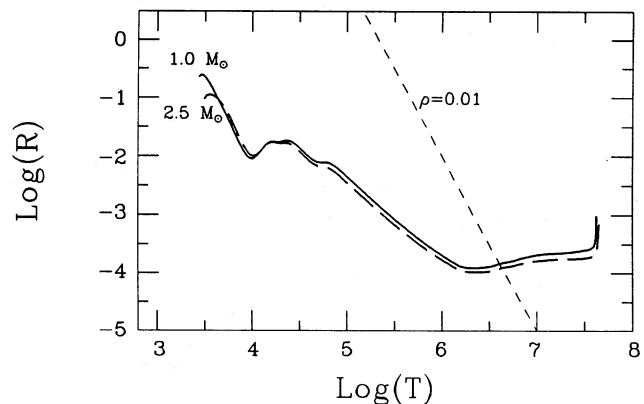


Figure 2. Plots of $\log(R)$ against $\log(T)$ for two red-giant models: $M = 1 M_\odot$, $\log(L/L_\odot) = 3.0105$, $\log(T_{\text{eff}}) = 3.4552$; and $M = 2.5 M_\odot$, $\log(L/L_\odot) = 3.2418$, $\log(T_{\text{eff}}) = 3.5089$. Both models are for stars with initial compositions of $X = 0.70$, $Z = 0.02$.

the adiabatic gradient, and not by equation (7) which involves the Rosseland mean opacity. In the convective region, knowledge of the Rosseland opacity is not of so much interest. For the other three models (2.5, 10 and 50 M_{\odot}), envelope convection does not occur and it is seen that, for a given model, R is approximately constant – at least to within an order of magnitude or so. For such stars, plots of opacities against $\log(T)$ for fixed values of $\log(R)$ give an impression of how the opacity varies with depth. Fig. 2 shows results for two red-giant models, omitting regions of degenerate cores. For those models $\log(R)$ shows larger variations as a function of $\log(T)$. Supergiants can have very small values of $\log(R)$, of -5 or less.

Use of the quantity $\log(R)$ is also convenient if, as in the OPAL work, one wishes to print rectangular tables of opacities; and it is convenient in making interpolations.

2 THE OPACITY PROJECT

The Opacity Project is an international collaboration concerned with the calculation of opacities for stellar envelopes. Work on equations of state (EOS) is described in four papers in the series ‘Equations of State for Stellar Envelopes’ (EOSSE) listed in Table 1. Work on the computation of atomic data is described in the series ‘Atomic Data for Opacity Calculations’ (ADOC) listed in Table 2.

We allow for plasma correlation effects in the work on equations of state (in order to obtain convergent partition functions) and in calculating the pressure-broadening of spectral lines. However, we make the assumption, valid for envelopes, that the initial states producing absorption are not significantly perturbed by the plasma environment (the exact procedures used are discussed in Section 5.4). A main objective of our work is to make extensive calculations of accurate atomic data. All of our atomic data will be made generally available: selected data in a book to be published by the Institute of Physics, and all data in a data base system *ropbase* (Cunto & Mendoza 1992). Implementation of *ropbase* at the Centre des Données Astronomiques de Strasbourg (CDS) is described by Cunto et al. (1993).

Hummer & Mihalas, in EOSSE I (see Table 1), tentatively adopt $\rho \leq 0.01$ for envelopes. That condition will be adopted here and will be discussed further in Section 5.4. With that condition, envelopes are the regions to the left of the dashed lines marked ‘ $\rho = 0.01$ ’ in Figs 1 and 2.

Table 1. Papers in the series ‘Equations of State for Stellar Envelopes’ (EOSSE), published in the *Astrophysical Journal*.

- I Hummer D. G., Mihalas D., 1988, An occupation probability formalism for the truncation of the internal partition function, *ApJ*, 331, 794
- II Mihalas D., Däppen W., Hummer D. G., 1988, Algorithms and selected results, *ApJ*, 331, 815
- III Däppen W., Mihalas D., Hummer D. G., Mihalas B. W., 1988, Thermodynamic quantities, *ApJ*, 332, 261
- IV Mihalas D., Hummer D. G., Mihalas B. W., Däppen W., 1990, Thermodynamic quantities and selected ionization fractions for six elemental mixes, *ApJ*, 350, 300

3 EQUATIONS OF STATE

In this section we use the indices i for the energy level, j for the ionization stage and k for the chemical element. We take the energies E_{ijk} to be increasing in order of increasing i . We define the ionization stage j to be such that an ion at stage j has a net charge of $z_j = j - 1$: then the neutral atom has $j = 1$ and charge zero, and the fully ionized atom has $j = Z_k + 1$ and charge Z_k , the nuclear charge. The index j is numerically equal to the Roman numeral used in spectroscopic notation. Number densities are N_{ijk} for level ijk ; $N_{jk} = \sum_i N_{ijk}$ for ionization stage jk ; $N_k = \sum_j N_{jk}$ for element k ; and $N = \sum_k N_k$ for the total number of nuclei. The electron density is

$$N_e = \sum_j z_j \sum_k N_{jk}. \quad (18)$$

Table 2. Papers in the series ‘Atomic data for Opacity Calculations’ (ADOC), published in the *Journal of Physics B (Atomic, Molecular and Optical Physics)*.

- I Seaton M. J., 1987, General formulation, *J. Phys. B*, 20, 6363
- II Berrington K. A., Burke P. G., Butler K., Seaton M. J., Storey P. J., Taylor K. T., Yan Y., 1987, Computational Methods, *J. Phys. B*, 20, 6379
- III Yan Y., Taylor K. T., Seaton M. J., 1987, Oscillator strengths for C II, *J. Phys. B*, 20, 6399
- IV Yan Y., Seaton M. J., 1987, Photoionization cross sections for C II, *J. Phys. B*, 20, 6409
- V Seaton M. J., 1987, Electron impact broadening of some C III lines, *J. Phys. B*, 20, 6431
- VI Thornbury J. F., Hibbert A. H., 1987, Static dipole polarisabilities of the ground states of the helium sequence, *J. Phys. B*, 20, 6447
- VII Fernley J. A., Taylor K. T., Seaton M. J., 1987, Energy-levels, f -values and photoionization cross sections for He-like ions, *J. Phys. B*, 20, 6457
- VIII Seaton M. J., 1988, Line-profile parameters for 42 transitions in Li-like and Be-like ions, *J. Phys. B*, 21, 3033
- IX Peach G., Saraph H. E., Seaton M. J., 1988, The lithium iso-electronic sequence, *J. Phys. B*, 21, 3669
- X Luo D., Pradhan A. K., Saraph H. E., Storey P. J., Yan Y., 1989, Oscillator strengths and photoionization cross sections for O III, *J. Phys. B*, 22, 389
- XI Luo D., Pradhan A. K., 1989, The carbon iso-electronic sequence, *J. Phys. B*, 22, 3377
- XII Seaton M. J., 1989, Line-profile parameters for neutral atoms of He, C, N and O, *J. Phys. B*, 22, 3603
- XIII Seaton M. J., 1990, Line profiles for transitions in hydrogenic ions, *J. Phys. B*, 23, 3255
- XIV Tully J. A., Seaton M. J., Berrington K. A., 1990, The beryllium sequence, *J. Phys. B*, 23, 3811
- XV Sawey P. M. J., Berrington K. A., 1992, Fe I to IV, *J. Phys. B*, 25, 1451
- XVI Saraph H. E., Storey P. J., Taylor K. T., 1992, *Ab initio* calculations for Fe VIII and Fe VII, *J. Phys. B*, 25, 4409
- XVII Burke V. M., 1992, Calculation of line-broadening parameters and collision strengths between $n = 2, 3$ and 4 states in C IV, *J. Phys. B*, 25, 4917
- XVIII Nahar S. N., Pradhan A. K., 1993, Photoionization cross sections and oscillator strengths for Si-like ions, $\text{Si}^0, \text{S}^{2+}, \text{Ar}^{4+}, \text{Ca}^{6+}$, *J. Phys. B*, 26, 1109
- XIX Butler K., Mendoza C., Zeippen C. J., 1993, The magnesium iso-electronic sequence, *J. Phys. B*, 26, 4409
- XX Nahar S. N., Pradhan A. K., 1994, Photoionization cross sections and oscillator strengths for Fe II, *J. Phys. B*, in press

3.1 A modified Boltzmann distribution

The essential difficulty in obtaining equations of state for ionized gases arises from the fact that the Coulomb potential gives rise to an infinite number of energy levels. The high levels have large mean radii which eventually become larger than typical interparticle separations in the plasma. Some cut-off procedures must therefore be introduced.

The procedure used in our work is to introduce *occupation probabilities*. Omitting the subscript k , the number density of atoms in level i for ionization stage j is taken to be

$$N_{ij} = N_j g_{ij} W_{ij} \exp(-E_{ij}/kT) / P_j, \quad (19)$$

where g_{ij} is a statistical weight, W_{ij} the occupation probability, E_{ij} the energy of the level and P_j the partition function,

$$P_j = \sum_i g_{ij} W_{ij} \exp(-E_{ij}/kT). \quad (20)$$

The W_{ij} go to zero for the higher states, which ensures that the summation in (20) is convergent. High states, with very small values of W_{ij} (values effectively zero), are said to be *dissolved*.

The procedures used for calculating the W_{ij} are discussed in EOSSE I. They are closely related to those for determining the line profiles. The levels become completely dissolved at the point where the lines in a series become completely blended.

We discuss the case of a hydrogenic ion of charge Z . In EOSSE I, Hummer & Mihalas consider the ion microfield, F , to be the main perturbation leading to dissolution. They use a simple form of saddle-point theory to obtain a field, F_{sp} , such that bound states can exist only for $F < F_{sp}$. They adopt $F_{sp} = (I_n/4)^2/Z$, where $I_n = Z^2/n^2$ is the ionization energy in Rydbergs and F is in atomic units. They take $F_c = F_{sp}$ for $n = 1$ and 2. For the higher states, $n \geq 3$, they argue that Stark splitting is a more efficient mechanism leading to dissolution, and use the criterion that dissolution of level n occurs when the highest Stark component of level n (calculated using first-order perturbation theory) has an energy equal to that of the lowest component of level $n + 1$. Correcting a minor error in EOSSE I (see ADOC XIII in Table 2), this criterion gives $F_c(n) = Z^3(2n + 1)/[6n^4(n + 1)^2]$. Putting $F_c(n) = K(n) \times F_{sp}(n)$, which defines $K(n)$, one obtains $K(n) = (16/3)(n + 1/2)/(n + 1)^2$, giving $K(3) = 3.5/3$. Hummer & Mihalas make a small adjustment to obtain $K(3) = 1$, and finally adopt $F_c(n) = K(n) \times F_{sp}(n)$, where

$$K(n) = \begin{cases} 1 & \text{for } n \leq 3, \\ 16n/[3(n + 1)^2] & \text{for } n \geq 3. \end{cases} \quad (21)$$

The occupation probability $W(n)$ is taken to be the probability of finding a microfield with $F < F_c(n)$,

$$W(n) = \int_0^{F_c(n)} P(F) dF, \quad (22)$$

where $P(F)$ is the microfield distribution, normalized to $\int_0^\infty P(F) dF = 1$. Using a Holtsmark distribution, Hummer & Mihalas show that a good approximation to (22) is given by

(using any consistent choice of units)

$$W_{ij} = \exp \left\{ -\frac{64\pi}{3} \left[\frac{(z_j + 1)^{1/2} e^2}{K_{ij}^{1/2} I_{ij}} \right]^3 Q N_e \right\}, \quad (23)$$

where

$$Q = (1/N_e) \sum_j z_j^{3/2} \sum_z N_{jk}. \quad (24)$$

For non-hydrogenic systems, n is replaced by the effective quantum number ν_{ij} for the state ij .

We have defined W_i to be the probability that level i is *occupied*; $(1 - W_i)$ is the probability of its being *dissolved*.

3.2 The ionization equilibrium

Our approach to determining ionization equilibria is discussed in EOSSE II. On minimizing the free energy one obtains¹

$$\ln \left(\frac{N_{j+1}/P_{j+1}}{N_j/P_j} \right) + \frac{I_j}{kT} + \eta + \phi_j = 0. \quad (25)$$

It is assumed here that the energies E_{ij} in (20) are relative to the ground state for ion j . The I_j in (25) are then ionization potentials from the ground state of j to that of $(j + 1)$. We use calculated excitation energies E_{ij} but, whenever available (Moore 1970), experimental ionization potentials.

In (25), η is the usual electron-degeneracy parameter defined by

$$F_{1/2}(\eta) = \frac{\sqrt{\pi}}{2} \frac{N_e}{P_e}, \quad (26)$$

where

$$P_e = 2 \left[\frac{mkT}{2\pi\hbar^2} \right]^{3/2} \quad (27)$$

and

$$F_k(\eta) = \int_0^\infty \frac{t^k dt}{\exp(t - \eta) + 1}. \quad (28)$$

In the non-degenerate limit of $N_e \ll P_e$, the solution of (26) is

$$\eta = \ln(N_e/P_e) \quad (\eta \ll 0). \quad (29)$$

In (25), ϕ_j allows for Coulomb interactions of free charged particles. It is proportional to $v^{3/2}$, where

$$v = e^2 N_e^{1/3} / (kT). \quad (30)$$

If $N_e^{-1/3}$ is taken to be the mean separation between the electrons, then v is equal to the ratio of the Coulomb electron-electron energy to the thermal energy. At low densities, v and ϕ_j are small.

The quantity ϕ_j depends on the chemical mixture through two ratios,

$$R = (1/N_e) \sum_j z_j^2 \sum_k N_{jk} \quad (31)$$

¹We use \ln for \log_e and \log for \log_{10} .

and

$$S = (N/N_e). \quad (32)$$

The expression adopted for ϕ_j , from Graboske, Harwood & Rogers (1969), is

$$\phi_j = -v^{3/2} \times \frac{2\sqrt{\pi} V^{3/2}}{3(1+x)} \left[\frac{3}{2V} (H_{-1/2} + 2z_j + 1) + X(2 - H_{3/2}/H_{1/2}) \right], \quad (33)$$

where

$$H_k(\eta) = d \ln[F_k(\eta)]/d\eta, \quad (34)$$

$$V = H_{1/2} + R, \quad (35)$$

$$x = \frac{4\sqrt{\pi}}{3} \frac{H_{3/2}}{S} V^{1/2} v^{3/2} \quad (36)$$

and

$$X = 3 \left\{ 1 - \frac{3}{x^3} (1+x) \left[\ln(1+x) - x + \frac{x^2}{2} \right] \right\} \quad (37)$$

$$= 9 \sum_{p \geq 1} \frac{(-x)^p}{(p+2)(p+3)}.$$

We note that ϕ_j is a linear function of j , $\phi_j = \alpha + \beta j$, a relation that is useful for computational work.

At lower densities we can omit the term in ϕ_j and use (29) for η . We then obtain an equation of familiar Saha-type,

$$\ln \left[\frac{(N_{j+1}/P_{j+1})(N_e/P_e)}{(N_j/P_j)} \right] + \frac{I_j}{kT} = 0. \quad (38)$$

3.3 The dependence of ionization equilibria on the chemical mixture

The ionization equilibria depend on the chemical mixture through the three ratios Q , R and S defined by (24), (31) and (32). For conditions in stellar envelopes, we find the equilibria to be insensitive to the exact values of these ratios. The reasons for this are that (i) the partition functions are insensitive to the exact values used for the occupation probabilities, and (ii) the term in ϕ_j is not of major importance and is not very sensitive to the exact values of the ratios R and S . We can therefore obtain a good approximation by taking the equilibria to depend only on temperature T and electron density N_e . This provides a major simplification for our work (see Section 5).

3.4 Electron density and mass density

We define

population fractions	$F_{ijk} = N_{ijk}/N_k$,
ion fractions	$F_{jk} = N_{jk}/N_k$,
electrons per atom	$\mathcal{E}_k = \sum_j z_j F_{jk}$,
chemical abundance fractions	$A_k = N_k/N$.

With these definitions the electron density is

$$N_e = \sum_k \mathcal{E}_k N_k = N \sum_k \mathcal{E}_k A_k, \quad (39)$$

and the mass density is

$$\rho = \sum_k M_k N_k = N \sum_k M_k A_k, \quad (40)$$

where M_k is the mass of atom k . Eliminating N ,

$$\rho = N_e \times \left(\sum_k M_k A_k \right) / \left(\sum_k \mathcal{E}_k A_k \right). \quad (41)$$

With our assumption that \mathcal{E}_k depends only on T and N_e , equation (41) gives the mass density for any assumed values of T , N_e and chemical composition.

4 ATOMIC DATA

Details of the atomic physics work in the Opacity Project are given in the ADOC series of papers (Table 2). A full summary will be given in a concluding paper of that series. A brief summary is given here.

4.1 Atomic wave functions

The wavefunction for one electron in a central potential is

$$\phi = \chi_{m_i}(\sigma) Y_{l m_i}(\hat{r})(1/r) P_{nl}(r), \quad (42)$$

where σ is the spin coordinate and (\hat{r}, r) the space coordinates. For N electrons we use \mathbf{x}_i for the coordinates (σ, \hat{r}, r) , and j for the set of quantum numbers $(nlm_i m_s)_j$. An antisymmetric wavefunction Φ_k is constructed using the determinant formed from the functions $\phi_j(\mathbf{x}_i)$. An approximate atomic wavefunction is

$$\Psi = \sum_k \Phi_k c_k. \quad (43)$$

A configuration is a set of $\{nl\}$ quantum numbers. Equation (43) gives a *configuration-interaction* (CI) wavefunction if the sum includes states of more than one configuration.

The energy $E = (\Psi|H|\Psi)$, where H is the Hamiltonian operator, must be minimized. This is achieved using CI codes, which determine the coefficients c_k and optimize the functions $P_{nl}(r)$. We use two CI codes, CIV3 by Hibbert (1975) and SUPERSTRUCTURE by Eissner & Nussbaumer (1969); a later version of SUPERSTRUCTURE, developed by Nussbaumer & Storey (1978) in Zurich, will be referred to as zss.

For the opacity work we consider states with $(N+1)$ electrons in which N electrons are more or less tightly bound and one added electron may be in a highly excited state or in the continuum (for a final state after photoionization). In the close coupling (CC) approximation, the complete wavefunction is taken to be

$$\Psi = \mathcal{A} \sum_i \psi_i \theta_i + \sum_j \Phi_j c_j, \quad (44)$$

where ψ_i is a CI function for N electrons, θ_i is a function for the added electron, \mathcal{A} is an antisymmetrization operator, and

the Φ_j are determinantal functions for the $(N+1)$ -electron system. In the language of atomic collision theory, the ψ_i are referred to as ‘target states’, and the states i are referred to as ‘channels’. The functions θ_i and coefficients c_j are fully optimized, using the R -matrix techniques described in ADOC II.

Consider, as an example, the case of $N=6$. The N -electron system has a ground configuration $1s^22s^22p^2$. The *ground complex* is defined as the set of configurations that have the same set of $\{n\}$ quantum numbers as the ground state. Thus for $N=6$ the ground complex includes the configurations $2s^22p^2$, $2s2p^3$ and $2p^4$, giving 12 energy levels in LS coupling. For a highly ionized system, all states of the ground complex are tightly bound. For the case of $N=6$ there is no difficulty in including all 12 of those levels in (44).

Now consider a more complicated case of $N=14$ with ground configuration $1s^22s^22p^63s^23p^2$. The ground complex now includes 3d electrons, giving configurations such as $3s^23p3d$, $3s^23d^2$ right up to $3d^4$. The number of ground-complex levels is now very large, and one certainly cannot include all of them in (44). For such systems, our procedure is to make CC calculations including only a fairly small number of target states in (44), and to make supplementary CI calculations using zss; these calculations, which were performed by A. E. Lynas-Gray and P. J. Storey, give what we refer to as PLUS data.

We compute atomic data for all cosmically abundant elements (H, He, C, N, O, Ne, Na, Mg, Al, Si, S, A, Ca and Fe) in all stages of ionization. We include all levels for which the added electron has a quantum number $l_i \leq LMAX$, where $LMAX$ is such that states with $l_i > LMAX$ are close to being hydrogenic. Let ν_i be the effective quantum number for an electron in channel i . We include all levels with $\nu_i \leq 10$, where here i refers to the lowest target level included in (44).

The PLUS data are all for transitions between states belonging to configurations of the type $3s^x3p^y3d^z$, and for excitations from such configurations.

4.2 Radiative transitions

Radiative transition probabilities are proportional to the squares of reduced matrix elements, $(\Psi_f \| \mathbf{D} \| \Psi_i)^2$, where f and i refer to final and initial states and \mathbf{D} is the dipole operator. All detailed formulae required are given in ADOC I.

We calculate oscillator strengths and photoionization cross-sections for all transitions for which the lower state lies below the first ionization threshold. For less complex systems, with $N \leq 12$, our atomic radiative data are probably accurate to within about 10 per cent for most transitions, but larger errors will occur for sensitive cases involving a lot of cancellation. For more complex systems, $N > 12$, the accuracy may not be quite so good. The accuracy of our atomic data is discussed further in individual papers of the ADOC series.

4.3 Configuration-interaction effects

We compare the use of functions Ψ_f , Ψ_i obtained using the CC expansion (44) with the use of single-configuration (SC) functions Φ_f , Φ_i . The CC expansion gives functions Ψ involving linear combinations of many configurations. Each

such function may be given a label, depending on the configuration that gives the largest contribution.

(a) *Many-electron jumps*. Matrix elements of the type $(\Phi_f \| \mathbf{D} \| \Phi_i)$ are non-zero only if the initial and final configurations differ in the nl quantum number of just one electron, and hence only one electron jumps. The matrix elements $(\Psi_f \| \mathbf{D} \| \Psi_i)$ can, however, be non-zero when the labels for the initial and final states differ in the nl values of more than one electron. These are described as ‘many-electron jumps’. The total number of lines in the CC approximation can be a good deal larger than the number in the SC approximation.

(b) *Accuracy of radiative data*. For many individual transitions in complex atoms, use of the SC approximation can give radiative data in error by factors of 2 or more.

(c) *Autoionization*. Most of the photoionization cross-sections obtained using the CC approximation contain complicated resonance structures. These are due to transitions to quasi-bound states that lie above the ionization limit, followed by autoionization.

4.4 Line profiles

Line broadening is produced by thermal Doppler effects, radiation damping and pressure effects. The atomic lifetimes required to calculate radiation-damping profiles are obtained from the calculated oscillator strengths. Pressure broadening is produced by both ions and electrons. For line profiles we use the notation $\phi(x)$, where $x = |\omega - \omega_0|$, ω being angular frequency and ω_0 the frequency at the line centre.

We follow the usual procedure of treating the ions in a quasi-static approximation, giving an ion microfield F with a distribution $P(F)$ normalized to $\int P(F) dF = 1$. Hydrogenic systems have levels nl degenerate with respect to l , giving linear Stark splittings in the microfield. For non-hydrogenic systems that degeneracy is broken and, for small values of F , the Stark splitting is quadratic. We make the somewhat drastic approximation of considering the microfield contribution only for true hydrogenic systems and, in a slightly modified form, for the resonance lines of He I. The line-broadening theory used for these systems, for both ion and electron perturbers, is described in detail in ADOC XIII. For Stark shifts we consider only microfields F smaller than the critical fields F_c introduced in Section 3.1. We then obtain profiles normalized to

$$\int_{-\infty}^{+\infty} \phi(x) dx = W(\text{upper}), \quad (45)$$

where $W(\text{upper})$ is the occupation probability for the final, upper, level.

For non-hydrogenic systems we consider only broadening by electrons, in the impact approximation. This approximation gives Lorentz profiles

$$\phi(x) = (\gamma/\pi) \{x^2 + \gamma^2\}^{-1}, \quad (46)$$

where $\gamma = N_e \Gamma$ and Γ is an atomic constant. Equation (46) gives profiles normalized to

$$\int_{-\infty}^{+\infty} \phi(x) dx = 1. \quad (47)$$

The constants Γ have been calculated (see ADOC VIII) for 42 transitions using a CC approximation, and the results obtained have been used to obtain an approximate formula that can be used for other transitions. Further work has been done by V. M. Burke (ADOC XVII) for transitions in C IV; an increase in the number of channels included in (44) gives improved agreement with the approximate formula.

Line profiles for neutral atoms are discussed in ADOC XII.

4.5 Fine structure

All of our main atomic data calculations are made neglecting relativistic effects. Inclusion of fine structure can lead to significant increases in opacity, particularly for low densities giving narrow lines. One is concerned with very large numbers of lines and even larger numbers of fine-structure components. It is not important to have exact values for the splittings, and for the distribution of oscillator strengths among the components. We therefore use approximate formulae, valid for one electron moving in a central potential. Neglecting fine structure the levels have quantum numbers nSL , and with fine structure they have $nSLJ$. The fine-structure splittings, due to spin-orbit interaction, are taken to be

$$\delta E(nSLJ) = \alpha(nSL)[J(J+1) - L(L+1) - S(S+1)]. \quad (48)$$

We use average values of the spin-orbit parameters $\alpha(nSL)$ from available experimental data. The oscillator strengths for the fine-structure components are

$$f(n'SL'J', nSLJ) = f(n'SL', nSL) \times (2L+1)(2J'+1) W^2(L'LJ'J; 1S), \quad (49)$$

where $W(L'LJ'J; 1S)$ is a Racah coefficient. It follows from (49) that

$$\sum_{J'J} f(n'SL'J', nSLJ)(2J+1) = f(n'SL', nSL)(2S+1)(2L+1). \quad (50)$$

In this approach we do not allow for intercombination lines, which involve a change in the spin quantum number S .

4.6 Iron-group elements

An appreciable fraction of our total computational effort has gone into calculating atomic data for iron. Other iron-group elements (Cr, Mn and Ni) have abundances much lower than that of iron but can still make significant contributions to the Rosseland mean opacities. This is because these elements contribute to monochromatic opacities at frequencies at which the contributions from all other elements are small. We cannot afford to compute atomic data for Cr, Mn and Ni of an accuracy comparable to that of the iron data. Instead, we use extrapolations from the iron data along iso-electronic sequences. This probably gives results of adequate accuracy.

4.7 Other contributions for H and He

We include three further contributions to opacities for H and He which are important at low temperatures, such that these two elements are mainly neutral.

Rayleigh scattering. This will be discussed further in Appendix C.

H⁻ bound-free transitions. We use the cross-section of Wishart (1979) which should be accurate to within about 1 per cent.

Electron-hydrogen and electron-helium free-free transitions. For free-free transitions we use data from Stille & Callaway (1970) for H, which are in good agreement with later data from Bell & Berrington (1987), and for He we use data from Bell, Berrington & Croskery (1982).

4.8 Accuracy of atomic data

Our calculations are optimized for positive ions. For all systems with $N \leq 12$ (that is to say up to and including the sequence of aluminium-like ions) we include, as target states, all states belonging to ground complexes. For all positive ions in these systems we estimate that our oscillator strengths and photoionization cross-sections should be accurate to about 10 per cent, except for sensitive cases involving a lot of cancellation. The accuracy may be less good for some neutral atoms that have low-lying target states not belonging to ground complexes. The accuracy may also be less good for systems with $N > 12$.

A comprehensive study of f -values for the ions C III, N IV and O V has been made by Allard et al. (1990), who considered all available calculated and experimental data. This study confirms our accuracy estimate. Further extensive compilations are being prepared at the US National Institute of Standards and Technology (NIST). A first volume, for all ions of C, N and O, will soon be published (Wiese, Deters & Fuhr 1994). Again, these compilations confirm our accuracy estimates for positive ions, but find some errors larger than 10 per cent in our data for some transitions in C I and N I. More than 90 per cent of all recommended data in the new NIST compilations are from the *or* work.

The atomic data used in the present work for the first few ionization stages of iron are not of high accuracy. Improved atomic data are being calculated for these ions and will be used in later opacity work. New results for Fe II are given by Le Dourneuf, Nahar & Pradhan (1993) and by Nahar & Pradhan in ADOC XX.

5 MONOCHROMATIC AND MEAN OPACITIES

5.1 Monochromatic opacities

The full expression for the monochromatic opacity of a mixture is

$$\kappa(u) = \left[\sum_{ijk} N_{ijk} \sigma_{ijk}(u) + \sum_{jk} N_{jk} N_e \tau_j(u) \right] \times [1 - \exp(-u)] + N_e \sigma_e(u), \quad (51)$$

where $[1 - \exp(-u)]$ is a correction factor for stimulated emission, $\sigma_{ijk}(u)$ is the total cross-section for absorption from level ijk (both lines and photoionization), $N_e \tau_j(u)$ is a cross-section for free-free transitions, and $\sigma_e(u)$ is a cross-section for electron scattering. We use a hydrogenic approximation for free-free transitions, with Gaunt factors from Hummer (1988a) (see also Storey & Hummer 1991). We use $\sigma_e(u)$ from Boercker (1987) with a relativistic correction. At low temperatures and densities, $\sigma_e(u)$ reduces to the Thomson cross-section σ_T . For the special cases of H and

He, one must include in (51) the contributions from the additional processes discussed in Section 4.7.

We put

$$\kappa(u) = \sum_k N_k \sigma_k(u) = N \sum_k A_k \sigma_k(u), \quad (52)$$

where $\sigma_k(u)$ is a total effective cross-section for element k . Using the definitions of F_{ijk} , F_{jk} and \mathcal{E}_k from Section 3.4, we obtain

$$\sigma_k(u) = \left[\sum_{ij} F_{ijk} \sigma_{ijk}(u) + \sum_j F_{jk} N_e \tau_j(u) \right] \times [1 - \exp(-u)] + \mathcal{E}_k \sigma_c(u). \quad (53)$$

We use a number, $NTOT$, of values of u in the range of u required for the calculation of mean opacities (say $0 \leq u \leq 20$). In order to resolve all of the lines it may be necessary to take $NTOT$ as large as 10^6 or more. We can, however, obtain accurate values for the means using a smaller number of points and trapezoidal-rule integrations – the technique is that of *opacity sampling*. We find that the differences in the means using 10^5 and 10^6 points are always much less than 1 per cent, and that the errors in using $NTOT=10^4$ are never larger than about 2 or 3 per cent. Production work is carried out with $NTOT=10^4$.

Having calculated $\sigma_k(u)$ on a mesh of $NTOT$ points u_n , we pack the data on to a smaller number of points u_m . These are chosen to be such that linear interpolations from the points u_m back to the points u_n give errors not larger than some specified fractional amount $DPACK$ (usually taken to be 0.01 or 0.02): since those errors are not systematic, the resulting errors in the mean opacities will be much smaller than $DPACK$.

We consider three temperature–density meshes: a fine mesh, F, with $\delta \log(T) = 0.025$, $\delta \log(N_e) = 0.25$; a medium mesh, M, with $\delta \log(T) = 0.05$, $\delta \log(N_e) = 0.5$; and a coarse mesh, C, with $\delta \log(T) = 0.1$, $\delta \log(N_e) = 1.0$. Using means calculated on the M mesh, and cubic interpolations, we can reproduce results calculated on the F mesh with errors not exceeding 1 or 2 per cent, and generally much smaller. The C mesh is used only for exploratory calculations.

For each temperature and electron density and each element k , we archive information on ionization equilibria and numbers of electrons per atom, \mathcal{E}_k ; Planck-mean cross-sections,

$$\sigma_{p,k} = \int f_p(u) \sigma_k(u) du; \quad (54)$$

and packed cross-sections, $\sigma_k(u_m)$.

5.2 Mean opacities

We define a chemical mixture by a set of abundances A_k , $\sum_k A_k = 1$. For each temperature and electron density we read the archived values of \mathcal{E}_k and calculate total number densities N and mass densities ρ using (39) and (40). We read the packed cross-sections $\sigma_k(u_m)$, interpolate back to the original, common mesh u_n and calculate the monochromatic opacity of the mixture using (52). We then evaluate the

integral for the calculation of the Rosseland mean. The Planck mean is

$$\kappa_p = N \sum_k A_k \sigma_{p,k}. \quad (55)$$

We have examined the combined errors that result from choices of frequency mesh, packing, and interpolation in T and N_e . Using $NTOT=10^4$, $DPACK=0.02$ and the M mesh for temperatures and densities, the final errors are never significantly larger than 3 per cent and are generally much smaller.

5.3 Smoothing of results for Rosseland means

The errors that arise from the use of opacity sampling are not of importance in themselves, since we do not claim an accuracy of better than 2 or 3 per cent in our results for κ_R . Those errors can, however, vary irregularly from one (T, ρ) tabular point to the next and hence produce much larger errors in the calculated derivatives,

$$\left. \frac{\partial \kappa_R}{\partial T} \right|_{\rho} \quad \text{and} \quad \left. \frac{\partial \kappa_R}{\partial \rho} \right|_T.$$

This problem arises with both OPAL and OP opacities.

Accurate values of the derivatives are required in astronomy. It would be prohibitively expensive to use much larger values of $NTOT$. An alternative procedure has been proposed by Seaton (1993), who showed that these difficulties can be overcome by using a modest amount of two-dimensional smoothing in the tables of $\kappa_R(T, \rho)$ before making interpolations and calculating derivatives.

5.4 Some further technical details

Further technical details concerning dissolved lines, Rayleigh scattering and far line-wings are given in Appendix C.

5.5 Allowance for plasma perturbations

We can now describe more precisely the extent to which we allow for plasma perturbations. All atomic data (energy levels, f -values and photoionization cross-sections) are calculated for free atoms. All level populations are calculated allowing for occupation probabilities. Bound–free contributions to opacities are calculated without allowance for plasma perturbations, except that some below-threshold extrapolations are made to regions of blended lines. Free–free contributions are included without any allowance for plasma perturbations. For bound–bound contributions we allow for broadening of both initial and final levels. For the upper states the effects of broadening may be large, leading to blending of the lines; we allow for contributions from dissolved lines, following the procedures discussed in Appendix A. For electron scattering we use the theory of Boercker (1987), which allows for correlation effects.

Let N_T be the total density of all particles in a plasma, and define a mean interparticle separation r_p by

$$\frac{4\pi}{3} r_p^3 N_T = 1. \quad (56)$$

Considering the case of fully ionized H and He with an abundance ratio $N(\text{He})/N(\text{H})=0.1$, we obtain

$$r_p = 1.18/\rho^{1/3}, \quad (57)$$

with r_p in atomic units and ρ in g cm^{-3} . Plasma perturbations will not be of major importance for systems with mean radii small compared with r_p .

With $\rho=0.01$, equation (57) gives $r_p=5.48$ atomic units. Consider a bound electron having an effective quantum number ν ($\nu=n-\mu$, where n is the principal quantum number and μ is the quantum defect), in the field of an ion with net charge ζ . We take $r_\nu = \nu^2/\zeta$ to be a typical radius of this state. Putting $r_\nu = r_p$ we obtain $\nu=2.3$ for $\rho=0.01$ and $\zeta=1$, corresponding to a neutral atom. At $\rho=0.01$, however, we are usually concerned with more highly ionized systems. With $\zeta=6$ we obtain $\nu=5.7$. The dominant contributions to opacities come from states with ν no larger than about 3. We conclude that our approach should be valid for $\rho \leq 0.01$. Some of our calculations extend to densities $\rho > 0.01$, but may not be of high accuracy in such regions.

6 RESULTS FOR OPACITIES

6.1 The *OP* codes

All *OP* calculations for equations of state and opacities have been made twice: first in Urbana and in Columbus using CRAY-YMP machines at the National Center for Supercomputer Applications at the University of Illinois and the Supercomputer Center at the Ohio State University; and secondly in London using the IBM-3090 at the Rutherford and Appleton Laboratory. These two sets of calculations use the same input physics, but codes that are largely independent. Initial comparisons revealed – not unexpectedly – some errors in both sets of codes. After these had been corrected, a good agreement between the results was obtained, which gives us increased confidence in their being correct.

Comparisons between *OP* and *OPAL* results have also been of great value. The first such comparisons, made in the spring of 1991, showed that further *PLUS* data for iron-group elements were required in the *OP* work.

6.1.1 Range of temperatures and densities

We perform calculations for temperatures in the range $3.5 \leq \log(T) \leq 7.0$. We make no attempts to include molecular opacities, which may be important at lower temperatures, say $\log(T) < 4.0$.

We consider a range of densities such as to give opacities for R in a range somewhat larger than $-7 < \log(R) < -1$. As has already been stated, our results should be treated with caution for $\log(\rho) > -2$.

6.2 Element abundances

Compositions for stars are usually expressed as mass fractions X , Y and Z ($X+Y+Z=1$) for hydrogen, helium and ‘metals’ (all elements other than H and He), together with information on the relative abundances of the metal atoms. Opacities are required for many different chemical compositions. A feature of the *OP* work is that we can, rather easily, obtain opacities for any required composition.

Some years ago, uncertainties in abundances were often at least as large as those in opacities. Even over the past few years, while the work on new opacities has been in progress, there have been significant revisions of the best estimates for solar abundances. The compilation of Anders & Grevesse (1989, hereafter AG89) has been used extensively. Later revisions by a number of workers are summarized by Grevesse & Noels (1993) and Grevesse, Noels & Sauval (1992). Their recommended solar abundances – which will be referred to¹ as S92 – are given in Table 3 for all of the chemical elements included in our work. Compared with the AG89 abundances, those of S92 are in improved agreement with meteoric values. One of the biggest changes is in the iron abundance, with the 1992 value being some 30 per cent lower than the 1989 one, and in better agreement with meteoric data.

For the opacity work we require accurate values for the relative abundances of the iron-group elements, Cr, Mn, Fe and Ni. The values given in Table 3 are obtained using meteoric values within the iron group. These relative iron-group values are probably good for all astronomical objects since thermonuclear processes giving iron-group elements will probably always be much the same.

6.3 Dissemination of *OP* results

In the *OP* work the independent variables are temperature T and electron density N_e . For any given composition we produce tables which, for each T and N_e , give the mass density ρ and the Planck and Rosseland means κ_p and κ_R . The routine *OPFIT* by Seaton (1993) can be used to read these tables and to give mean opacities and their first two deriva-

Table 3. Best estimates of solar photospheric abundances, referred to as S92, from Anders & Grevesse (1989) together with later revisions from Grevesse & Noels (1992) and Grevesse, Noels & Sauval (1992). Values of $\log(A_k)$ are normalized to 12.00 for hydrogen.

k	$\log(A_k)$
H	12.00
He	11.00±0.02
C	8.55±0.05
N	7.97±0.07
O	8.87±0.07
Ne	8.07±0.06
Na	6.33±0.03
Mg	7.58±0.05
Al	6.47±0.07
Si	7.55±0.05
S	7.21±0.06
Ar	6.52±0.10
Ca	6.36±0.02
Cr	5.67±0.03
Mn	5.39±0.03
Fe	7.51±0.01
Ni	6.25±0.04

¹These abundances are close, but not identical, to those referred to as G91 in the *OPAL* work.

tives for any required values of T and ρ . It provides an option for smoothing (see Section 5.3) which gives improved accuracy for the derivatives. We can also produce tables in OPAL formats, i.e. opacities as functions of $\log(T)$ for fixed values of $\log(R)$.

In the present paper we do not give extensive printed tables of opacities since we believe that most users will prefer to have such data in computer-readable form. Requests for tables of OP opacities should be sent to one of the following addresses.

Dr A. E. Lynas-Gray, Astrophysics, Keble Road, Oxford OX1 3RH.

Telephone: +44-865-73363.

Electronic mail (INTERNET): aelg@oxds02.astro.ox.ac.uk.

Dr Anil K. Pradhan, Department of Astronomy, 174 W. 18th Av., The Ohio State University, Columbus, Ohio 43210-1106, USA.

Telephone: +614-292-5850.

Electronic mail (INTERNET): pradhan@seaton.mps.ohio-state.edu.

Users should specify whether they require original OP tables together with the code OPFIT, or results in OPAL formats. Abundances should be specified either as values of X and Z and some standard tabulation of relative metal abundances (such as AG89 or S92), or as number fractions, A_k , for all of the elements included in Table 3.

6.4 General description of OP results

We give one printed table in OPAL format for Rosseland mean opacities with S92 abundances (Table 4), together with results for other cases in graphical form. In this section we discuss some general trends, as illustrated by our results, and in Section 7 we make comparisons with results from other opacity calculations. In some of the plots shown in this subsection we include results from the OPAL work, which will be discussed further in Section 7.

Unless stated to the contrary, we include fine structure for iron and iron-group elements. We have not included fine structure for other elements, for which its effects will probably not be so large.

6.4.1 Hydrogen

Fig. 3 shows Rosseland mean opacities for hydrogen as functions of $\log(T)$ for $\log(R) = -1, -2, -3, -4, -5$ and -6 . There are two maxima, at about $\log(T) = 4.0$ and 4.7 . The first is due to H in excited states, the second to H in its ground state. The Rosseland weighting function $f_R(u)$ defined by (14) has a maximum value at $u_{\max} = 3.830\dots$, and u , defined by (11), is equal to $157887/T$ for a frequency corresponding to 1 Ry. Thus at $\log(T) = 4.0$ the Lyman limit is at $u = 15.79$ and absorption in the hydrogen Lyman continuum does not contribute significantly to the Rosseland mean. At $\log(T) = 4.7$ the Lyman limit has moved down to $u = 3.15$ and Lyman-continuum absorption is much more important. At higher temperatures the opacity decreases because the hydrogen becomes increasingly ionized. At the highest densities considered, for $\log(R) = -1$, the minimum between the two maxima has disappeared, giving only one maximum. This is due, at least in part, to the increase in the

breadth of the hydrogen Lyman lines with increasing density. Fig. 4 show the effects of an increase in density on the profiles of the Lyman lines. We consider $\log(T) = 4.3$ and two electron densities, $\log(N_e) = 16.0$ and 17.5 , corresponding to $\log(R) = -3.176$ and -1.126 .

Fig. 5 shows the effects of dissolution of the hydrogen ground state for the case of $\log(T) = 6.0$. There are three plots, all against $\log(\rho)$. The first shows the ground-state occupation probability, $W(1)$, which varies from unity at low densities to zero at high densities. By the time that $\log(\rho) = -2$ is reached, significant dissolution has already occurred. The second plot shows the fractional abundance of neutral hydrogen, H^0/H . Initially, this increases with increasing density, but the increase is eventually halted by ground-state dissolution. At $\log(T) = 6.0$, the maximum value of H^0/H is never larger than 2.2×10^{-3} . For many problems in work on EOS, such as the determination of specific heats, such small fractional abundances may not be of much importance. We have to consider whether they contribute to opacities. The third plot shows the ratio

$$r = \frac{\kappa_R(\text{including Lyman continuum})}{\kappa_R(\text{neglecting Lyman continuum})}. \quad (58)$$

It is seen that the build-up in H^0 produces an increase in opacity which is never larger than 6 per cent. The effect is therefore significant but not large. In order to improve the accuracy of our calculations it would be necessary to consider the optical properties of ground-state hydrogen atoms perturbed by the plasma environment.

6.4.2 Helium

Fig. 6 shows results for helium for $\log(R) = -1, -2, -3$ and -4 . There are three maxima due to He^0 in excited states, He^0 in its ground state and He^+ in excited states, and He^+ in its ground state.

6.4.3 Low metal abundances

Fig. 7 shows two plots for $\log(R) = -3$. The first is for $X = 0.7, Z = 0.0$ (implying $Y = 0.3$) and the second for $X = 0.7, Z = 0.001$. These are cases that may be of interest for studies of RR Lyrae stars. In the second plot we show, as a thin line, the results for $X = 0.7, Z = 0.0$. It is seen that the 'metals', even with abundances as low as 0.1 per cent by mass, make significant contributions to the opacity at higher temperatures.

6.4.4 Solar abundances

Opacities for $X = 0.7, Z = 0.02$ and S92 abundances are given in Table 4 and plotted in Fig. 8 for $\log(R) = -1, -2, -3, -4, -5$ and -7 . In general, there are four maxima. The first two are mainly due to H and He and have been discussed in Sections 6.4.1 and 6.4.2. The other two are mainly due to the 'metals'. The maximum at $\log(T) \approx 5.3$ is sometimes referred to as the 'Z-bump'; it is of particular importance for pulsation studies.

Fig. 9 shows, for the case of $\log(R) = -3$, the contributions from four different groups of elements. In producing these plots we consider for all cases the same chemical

Table 4. Rosseland mean opacities for $X=0.7$, $Z=0.02$ and S92 abundances. Values of $\log(\kappa_R)$ are presented with κ_R in $\text{cm}^2 \text{g}^{-1}$.

$\log(T)$	$\log(R) =$												
	-7.0	-6.5	-6.0	-5.5	-5.0	-4.5	-4.0	-3.5	-3.0	-2.5	-2.0	-1.5	-1.0
3.500	-4.172	-4.177	-4.180	-4.186	-4.197	-4.212	-4.216	-4.190	-4.120	-3.997	-3.815	-3.566	-3.264
3.550	-3.927	-4.019	-4.076	-4.102	-4.108	-4.095	-4.051	-3.956	-3.793	-3.560	-3.280	-2.981	-2.679
3.600	-3.299	-3.478	-3.641	-3.781	-3.889	-3.950	-3.942	-3.841	-3.627	-3.312	-2.940	-2.559	-2.194
3.650	-2.527	-2.747	-2.957	-3.154	-3.330	-3.473	-3.555	-3.551	-3.414	-3.144	-2.769	-2.345	-1.917
3.700	-1.773	-2.004	-2.231	-2.452	-2.652	-2.824	-2.935	-2.944	-2.862	-2.680	-2.425	-2.107	-1.730
3.750	-1.122	-1.330	-1.544	-1.756	-1.957	-2.122	-2.230	-2.248	-2.165	-2.012	-1.805	-1.566	-1.299
3.800	-0.679	-0.799	-0.947	-1.110	-1.269	-1.406	-1.489	-1.501	-1.436	-1.300	-1.123	-0.919	-0.696
3.850	-0.536	-0.535	-0.548	-0.588	-0.649	-0.704	-0.735	-0.727	-0.668	-0.567	-0.427	-0.260	-0.072
3.900	-0.524	-0.488	-0.420	-0.323	-0.218	-0.123	-0.048	0.021	0.092	0.178	0.281	0.407	0.554
3.950	-0.528	-0.493	-0.416	-0.276	-0.064	0.196	0.439	0.629	0.767	0.872	0.966	1.064	1.173
4.000	-0.526	-0.501	-0.433	-0.297	-0.065	0.259	0.629	0.974	1.236	1.419	1.551	1.654	1.750
4.050	-0.501	-0.488	-0.439	-0.322	-0.106	0.220	0.626	1.055	1.447	1.754	1.969	2.119	2.233
4.100	-0.482	-0.466	-0.423	-0.328	-0.144	0.154	0.549	0.999	1.456	1.875	2.205	2.439	2.601
4.150	-0.467	-0.451	-0.408	-0.317	-0.147	0.117	0.477	0.912	1.384	1.857	2.283	2.626	2.866
4.200	-0.456	-0.435	-0.395	-0.311	-0.153	0.099	0.442	0.853	1.310	1.793	2.272	2.702	3.038
4.250	-0.451	-0.427	-0.383	-0.303	-0.159	0.076	0.412	0.824	1.276	1.753	2.243	2.719	3.133
4.300	-0.445	-0.418	-0.374	-0.296	-0.155	0.071	0.395	0.807	1.271	1.753	2.240	2.730	3.198
4.350	-0.432	-0.401	-0.354	-0.277	-0.143	0.079	0.402	0.814	1.280	1.775	2.277	2.774	3.253
4.400	-0.424	-0.390	-0.336	-0.256	-0.127	0.086	0.407	0.826	1.303	1.807	2.321	2.832	3.326
4.450	-0.404	-0.370	-0.309	-0.219	-0.084	0.128	0.443	0.859	1.340	1.852	2.376	2.899	3.413
4.500	-0.389	-0.347	-0.277	-0.174	-0.028	0.189	0.506	0.921	1.401	1.915	2.445	2.978	3.503
4.550	-0.387	-0.346	-0.271	-0.147	0.029	0.263	0.582	0.994	1.471	1.983	2.516	3.054	3.587
4.600	-0.380	-0.337	-0.266	-0.138	0.064	0.345	0.694	1.105	1.571	2.069	2.591	3.127	3.659
4.650	-0.384	-0.344	-0.273	-0.148	0.062	0.368	0.762	1.208	1.675	2.159	2.659	3.176	3.696
4.700	-0.384	-0.347	-0.281	-0.161	0.045	0.353	0.753	1.218	1.712	2.207	2.700	3.197	3.695
4.750	-0.390	-0.351	-0.293	-0.187	0.005	0.304	0.703	1.167	1.667	2.181	2.685	3.178	3.661
4.800	-0.393	-0.360	-0.301	-0.200	-0.023	0.255	0.638	1.094	1.590	2.104	2.620	3.123	3.603
4.850	-0.395	-0.360	-0.305	-0.210	-0.042	0.220	0.580	1.023	1.514	2.027	2.544	3.054	3.543
4.900	-0.386	-0.353	-0.300	-0.212	-0.055	0.196	0.539	0.963	1.447	1.961	2.481	2.995	3.491
4.950	-0.374	-0.343	-0.291	-0.203	-0.053	0.185	0.519	0.934	1.407	1.916	2.440	2.957	3.456
5.000	-0.354	-0.325	-0.276	-0.193	-0.047	0.184	0.511	0.924	1.396	1.903	2.423	2.938	3.435
5.050	-0.302	-0.277	-0.234	-0.156	-0.017	0.208	0.529	0.934	1.401	1.903	2.419	2.930	3.422
5.100	-0.236	-0.205	-0.161	-0.090	0.039	0.252	0.562	0.958	1.417	1.911	2.422	2.923	3.397
5.150	-0.176	-0.136	-0.083	-0.009	0.115	0.314	0.608	0.993	1.444	1.930	2.426	2.908	3.351
5.200	-0.133	-0.075	-0.005	0.084	0.213	0.405	0.680	1.040	1.468	1.937	2.417	2.874	3.278
5.250	-0.136	-0.061	0.028	0.140	0.291	0.492	0.753	1.083	1.481	1.928	2.389	2.817	3.175
5.300	-0.179	-0.089	0.018	0.151	0.323	0.544	0.812	1.129	1.501	1.915	2.344	2.737	3.059
5.350	-0.244	-0.151	-0.035	0.111	0.300	0.539	0.824	1.145	1.503	1.892	2.286	2.641	2.934
5.400	-0.313	-0.232	-0.123	0.026	0.230	0.487	0.792	1.135	1.492	1.858	2.220	2.540	2.804
5.450	-0.377	-0.311	-0.215	-0.077	0.120	0.389	0.717	1.081	1.460	1.823	2.157	2.445	2.677
5.500	-0.418	-0.374	-0.299	-0.174	0.016	0.282	0.617	0.996	1.388	1.766	2.097	2.362	2.570
5.550	-0.441	-0.412	-0.361	-0.265	-0.101	0.147	0.486	0.887	1.300	1.686	2.025	2.286	2.479
5.600	-0.450	-0.432	-0.399	-0.332	-0.201	0.031	0.377	0.795	1.221	1.603	1.936	2.203	2.390
5.650	-0.455	-0.443	-0.421	-0.375	-0.275	-0.077	0.254	0.688	1.133	1.523	1.845	2.105	2.305
5.700	-0.456	-0.447	-0.431	-0.399	-0.327	-0.169	0.133	0.569	1.039	1.444	1.761	2.011	2.218
5.750	-0.458	-0.449	-0.437	-0.411	-0.355	-0.232	0.022	0.435	0.927	1.360	1.685	1.931	2.137
5.800	-0.459	-0.451	-0.440	-0.418	-0.371	-0.268	-0.056	0.317	0.805	1.265	1.610	1.860	2.069
5.850	-0.460	-0.453	-0.443	-0.423	-0.381	-0.293	-0.111	0.221	0.690	1.166	1.535	1.797	2.012
5.900	-0.459	-0.453	-0.443	-0.425	-0.386	-0.304	-0.139	0.159	0.601	1.078	1.462	1.738	1.963
5.950	-0.457	-0.451	-0.442	-0.425	-0.390	-0.314	-0.160	0.117	0.531	1.001	1.399	1.687	1.924
6.000	-0.453	-0.448	-0.439	-0.423	-0.390	-0.319	-0.173	0.090	0.482	0.937	1.340	1.644	1.894
6.050	-0.450	-0.442	-0.432	-0.416	-0.384	-0.319	-0.182	0.069	0.446	0.889	1.292	1.609	1.872
6.100	-0.449	-0.438	-0.426	-0.408	-0.377	-0.314	-0.185	0.052	0.416	0.850	1.253	1.580	1.849
6.150	-0.453	-0.439	-0.422	-0.398	-0.364	-0.303	-0.181	0.045	0.395	0.817	1.218	1.549	1.817
6.200	-0.458	-0.447	-0.427	-0.397	-0.354	-0.288	-0.172	0.041	0.377	0.790	1.187	1.511	1.774
6.250	-0.462	-0.455	-0.439	-0.408	-0.355	-0.276	-0.153	0.051	0.370	0.769	1.155	1.464	1.722
6.300	-0.464	-0.459	-0.450	-0.426	-0.373	-0.282	-0.143	0.067	0.373	0.751	1.114	1.407	1.646
6.350	-0.465	-0.462	-0.455	-0.440	-0.398	-0.305	-0.149	0.078	0.383	0.736	1.064	1.335	1.553
6.400	-0.466	-0.463	-0.459	-0.447	-0.417	-0.339	-0.178	0.067	0.378	0.710	1.000	1.244	1.449
6.450	-0.467	-0.464	-0.461	-0.453	-0.429	-0.368	-0.224	0.030	0.349	0.661	0.919	1.140	1.344
6.500	-0.467	-0.465	-0.462	-0.456	-0.437	-0.387	-0.264	-0.025	0.292	0.588	0.823	1.034	1.234
6.550	-0.467	-0.466	-0.464	-0.458	-0.442	-0.401	-0.298	-0.085	0.218	0.501	0.721	0.929	1.123
6.600	-0.468	-0.467	-0.465	-0.460	-0.447	-0.412	-0.325	-0.142	0.139	0.411	0.621	0.825	1.015
6.650	-0.469	-0.468	-0.466	-0.463	-0.452	-0.421	-0.345	-0.185	0.062	0.318	0.528	0.726	0.909
6.700	-0.470	-0.469	-0.467	-0.464	-0.455	-0.429	-0.365	-0.226	-0.007	0.229	0.436	0.633	0.802
6.750	-0.470	-0.469	-0.468	-0.466	-0.458	-0.436	-0.381	-0.263	-0.070	0.148	0.347	0.542	0.689
6.800	-0.470	-0.469	-0.469	-0.467	-0.461	-0.442	-0.396	-0.295	-0.129	0.070	0.265	0.446	0.599
6.850	-0.471	-0.470	-0.469	-0.467	-0.462	-0.447	-0.408	-0.323	-0.179	-0.001	0.188	0.354	0.520
6.900	-0.471	-0.471	-0.470	-0.467	-0.463	-0.451	-0.418	-0.346	-0.223	-0.063	0.117	0.271	0.451
6.950	-0.472	-0.472	-0.470	-0.468	-0.464	-0.453	-0.425	-0.364	-0.259	-0.114	0.050	0.199	0.388
7.000	-0.473	-0.473	-0.471	-0.469	-0.464	-0.453	-0.428	-0.377	-0.286	-0.155	-0.009	0.139	0.335

composition of $X=0.7$, $Z=0.02$ and S92 abundances, the different contributions being progressively 'switched on': apart from contributing to abundance fractions, the elements *not* 'switched on' are completely inert; they contribute neither to opacities nor to ionization equilibria. The four groups are (a) H and He; (b) H to Ne; (c) H to Ca; and (d) H to Ni. The elements C, N, O and Ne in group (b) give significant opacity enhancements, which are particularly important at the higher temperatures, $\log(T) \approx 6.3$, where they produce the fourth opacity maximum. The elements Na, Mg, Al, Si, S, Ar and Ca, included in group (c), give contributions that are particularly important in the region of $\log(T) \approx 5.9$, where the group (b) elements give a minimum. Finally, in group (d),

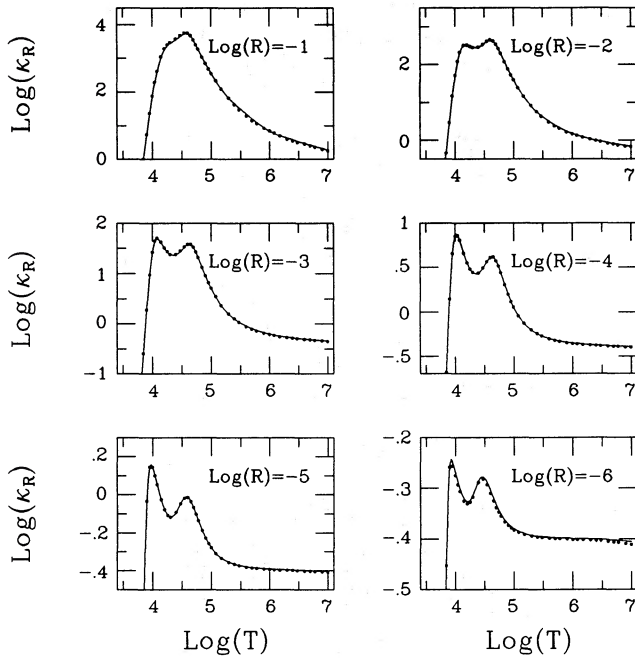


Figure 3. Opacities for hydrogen, for six values of $\log(R)$. OP results are shown by full lines and OPAL results by filled circles.

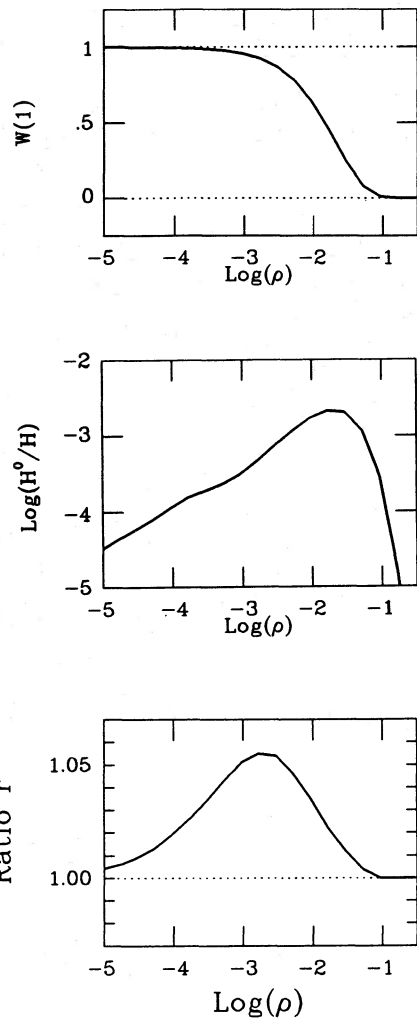


Figure 5. Effects of dissolution of the H ground state for the case of $\log(T) = 6.0$. Each of the three plots is against $\log(\rho)$. The top plot shows the ground-state occupation probability $W(1)$; the middle plot shows the fractional abundance of neutral H, H^0/H ; and the bottom plot shows the ratio r of Rosseland means with and without inclusion of the Lyman continuum.

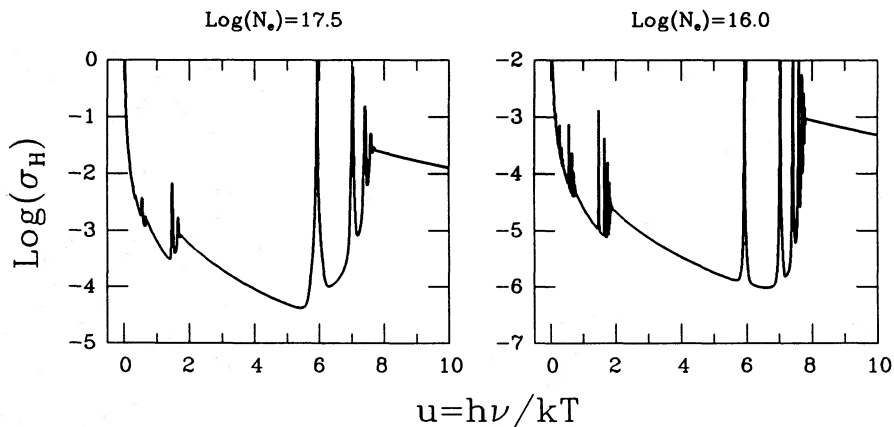


Figure 4. Opacity cross-section σ_H for hydrogen at $\log(T) = 4.3$ and $\log(N_e) = 16.0$ and 17.5 , corresponding to $\log(R) = -3.176$ and -1.126 . The cross-sections are in atomic units.

we include the iron-group elements which lead to further major enhancements, particularly in the region of the Z-bump.

Fig. 10 shows the complexity of the iron monochromatic opacities. We consider the case of $\log(T) = 5.3$, $\log(N_e) = 18$, corresponding to $\log(R) = -3.604$ for the S92 mix. For this plot we use 10^6 frequency points in the range $0 < u \leq 20$. The upper plot shows the cross-section σ for $0 \leq u \leq 10$. There are two lower plots: that on the left shows the region $4.9 \leq u \leq 5.1$ with lines just beginning to be resolved, and that on the right shows the region $4.99 \leq u \leq 5.01$ with all detail fully resolved. For normal production work it is not necessary to use such a high resolution – see Section 5.1.

In the region of the Z-bump there are very many lines due to iron ions in configurations of the type $3s^x 3p^y 3d^z$ and $3s^x 3p^y 3d^z nl$. Using PLUS data (see Section 4.1) we have checked the convergence of our calculations with respect to the inclusion of lines involving such configurations.

Unless stated to the contrary, whenever we include iron we also include the other three iron-group elements, Cr, Mn and Ni, and for all iron-group elements we include fine structure. Fig. 11 shows effects of including fine structure and Cr, Mn and Ni. The most important effects occur at low densities. For Fig. 11 we consider $\log(R) = -3$ and -5 , and the same mixture as that used for Fig. 9. For the left-hand

plots we ‘switch off’ the opacities of Cr, Mn and Ni and consider the increase in opacity that results from the inclusion of fine structure for iron. For the right-hand plots we consider the effects of including the other three elements. The effect of splitting the multiplets into fine-structure components is to give additional opacity in regions between the lines, as calculated neglecting fine structure. Although the combined abundances of Cr, Mn and Ni are less than 8 per cent of that of iron, their inclusion can lead to significant opacity enhancements. This is because these three elements give contributions to monochromatic opacities at frequencies where all other contributions are small. The combined effect of including fine structure and the other three iron-group elements is to increase the Rosseland mean by just over 80 per cent in the region of the Z-bump for $\log(R) = -5$.

6.4.5 Low temperatures

Our calculations extend down to $\log(T) = 3.5$, but will not be accurate at the lower temperatures because of our neglect of molecular contributions. We also neglect other effects, such as line broadening by neutral-neutral interactions. It will eventually be desirable to take the monochromatic atomic

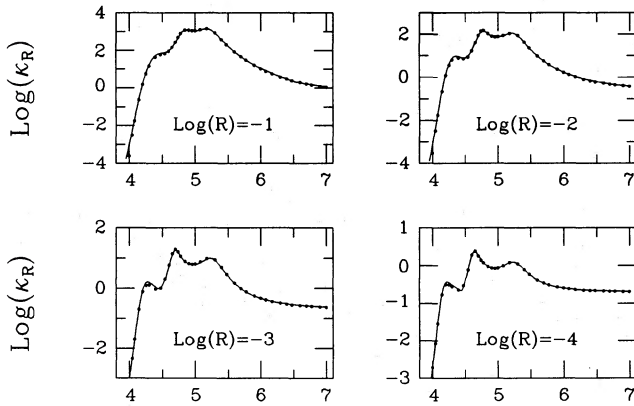


Figure 6. Opacities for helium, for four values of $\log(R)$. OP results are represented by full lines, OPAL results by filled circles.

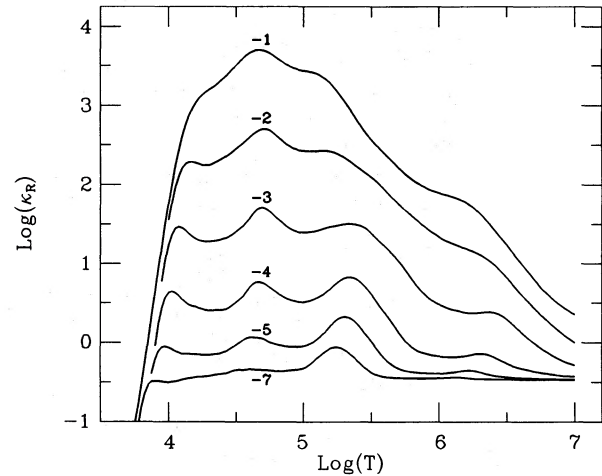


Figure 8. Opacities for $X=0.7$, $Z=0.02$ and S92 abundances. Results are given for $\log(R) = -1, -2, -3, -4, -5$ and -7 .

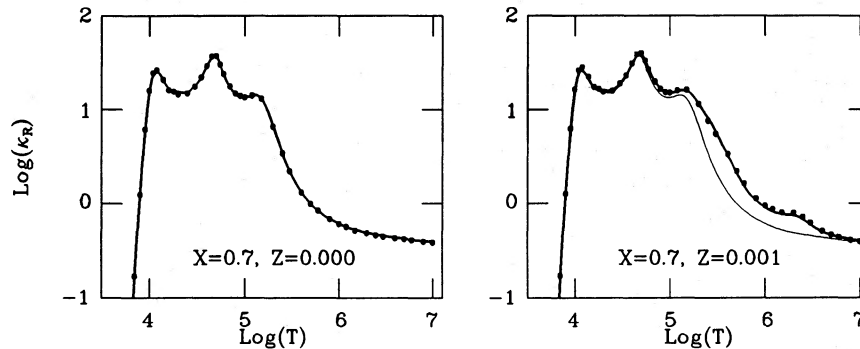


Figure 7. Two plots of opacities for $\log(R) = -3$. The left-hand plot is for $X=0.7$, $Z=0.000$, the right-hand one for $X=0.7$, $Z=0.001$. OP results are represented by full lines, OPAL results by filled circles. The thin line on the right-hand plot is for the case of the left-hand plot, $X=0.7$, $Z=0.000$.

opacities and add to them the contributions from molecules. In this way one should be able to obtain a smooth join of atomic opacities at higher temperatures and molecular opacities at lower values.

It is of interest to consider briefly the behaviour of the atomic opacities at low temperatures. In Fig. 12 we plot Rosseland means against $\log(R)$ for two values of $\log(T)$, 3.5 and 3.75. We consider four groups of contributions, as in Fig. 9. The lowest curves in Fig. 12 are for H and He only. There are important contributions from Rayleigh scattering. This process, considered on its own, gives a divergent Rosseland

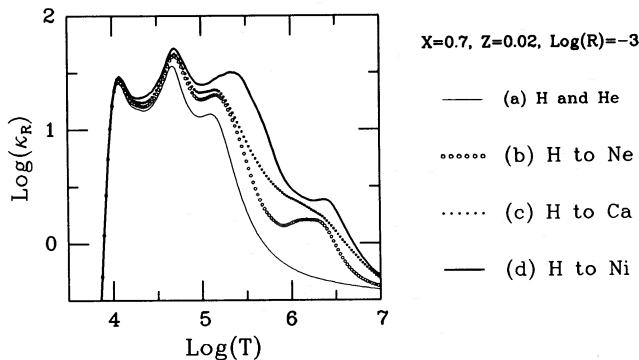


Figure 9. Contributions to opacities for $X=0.7$, $Z=0.02$, S92 abundances and $\log(R) = -3$. The same chemical composition is used throughout. The contributions to opacities from four different groups of elements are progressively 'switched on'.

integral: it is essential to include other processes, such as free-free transitions, which dominate for sufficiently small frequencies. It can be shown using equation (38) that the fractional abundance of H^- , $N(H^-)/N(H)$, increases with increasing density, which explains the behaviour of κ_R at the higher densities considered. On the other hand, the ratio $N(H^+)/N(H)$ increases with decreasing density (at sufficiently low densities the hydrogen becomes fully ionized even at these low temperatures). The Rosseland mean therefore increases at the lowest density and eventually approaches a value dominated by electron scattering.

For the case of $\log(T) = 3.5$, inclusion of the elements C to Ne produces little change. Dramatic enhancements occur on adding the next group, which includes the true metals Na, Mg, Al and Ca. These elements are significantly ionized even at such low temperatures and provide additional electrons for the formation of H^- . The iron-group elements give a further modest increase in the electron density at $\log(R) < -2$, but iron is mostly neutral at the higher densities.

For $\log(T) = 3.75$ the true metals are no longer of such importance at the lower densities, since ionization of H is now producing more electrons, but do lead to significant enhancements at the higher densities.

6.4.6 Some sensitivity studies

Cases for which single-element monochromatic opacities are small and sensitive to detailed treatments are discussed in

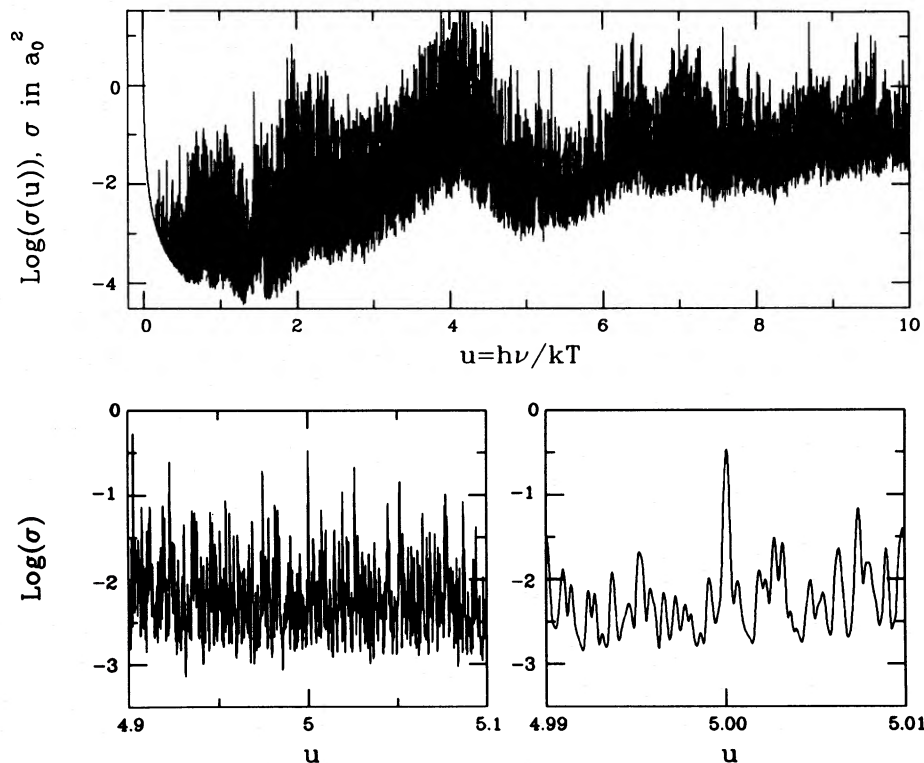


Figure 10. The opacity cross-section σ for iron, with $\log(T) = 5.30$, $\log(N_e) = 18.0$, and the EOS for a solar mix. For such a mix, the value of N_e used corresponds to the case of $\log(R) = -3.604$. The two lower plots show the results obtained using an increasingly more expanded frequency scale.

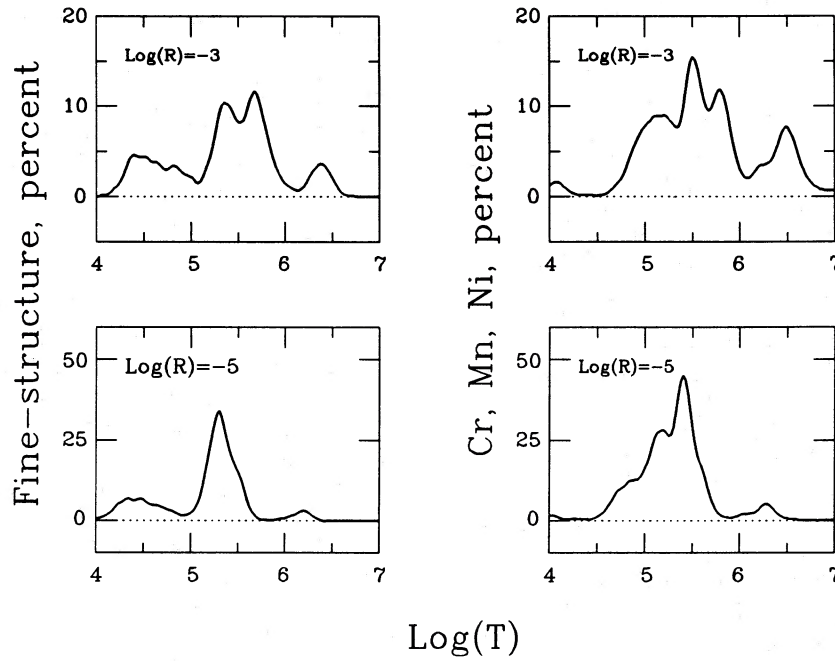


Figure 11. The sensitivity of opacity to the inclusion of fine structure (left-hand plots) and to the inclusion of the iron-group elements Cr, Mn and Ni (right-hand plots). The results are shown for $\log(R) = -3$ (upper plots) and $\log(R) = -5$ (lower plots) and the same chemical composition as that used for Fig. 8.

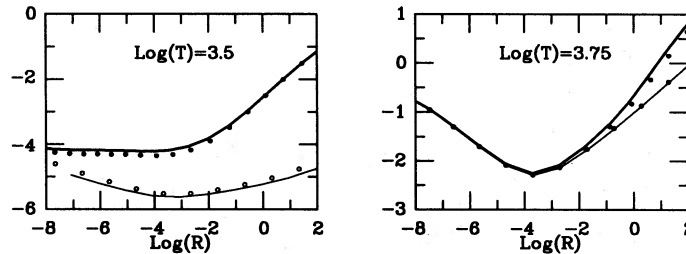


Figure 12. Opacities at low temperatures, $\log(T) = 3.50$ and 3.75 . Symbols for the groups of elements included are as in Fig. 9.

Appendix A, Section A3.3. We introduce a parameter *POPMIN* and include all excited states with fractional populations greater than *POPMIN*. Two sets of calculations have been made. In the first we use $POPMIN = 10^{-8}$ and omit the factor $(\omega/\omega_n)^4$ in (A21). In the second we use $POPMIN = 10^{-10}$ and include the factor $(\omega/\omega_n)^4$, which gives a reduction in the contributions from the far red-wings of lines. For single-element opacities we find significant differences between the Rosseland means from those two runs, in regions where these means are small. When we calculate opacities for mixtures, however, we find that these two sets of calculations give results that are almost exactly the same. This is because, in regions where the monochromatic opacity for any one element is small, other elements will come in and give larger contributions.

It is also necessary to consider the sensitivity to values adopted for the pressure-broadening parameters, γ , for the spectral lines. There is little sensitivity at high densities, where the lines become smeared out to give a quasi-continuum, or at low densities, where the profiles are mainly determined by Doppler broadening and radiation damping.

At intermediate densities the main quantity of interest is the frequency shift from the line centre, $\Delta\omega$, at which the line opacity reaches some specified fraction (say one-half) of the background continuum opacity. For the wings of Lorentz profiles we have $\Delta\omega \propto \sqrt{\gamma}$. A number of test calculations have been made with all values of γ increased by a factor of 2. In many cases we find that such changes in the values of γ do not lead to changes in the Rosseland means by more than a few per cent. There are, however, some sensitive cases. For example for a solar mix with $\log(T) = 5.2$ and $\log(N_e) = 15.5$, giving $\log(R) = -5.803$, we obtain a 33 per cent increase in the Rosseland mean on replacing γ by $2 \times \gamma$ for all iron lines.

7 COMPARISON WITH OTHER CALCULATIONS

7.1 Comparison with LAOL

Fig. 13 gives a comparison of LAOL and OP opacities, the former being interpolated from table WKM 10 of Weiss et al. (1990). We here consider $X = 0.7$, $Z = 0.02$ and the ‘Cox–Tabor’ relative abundances of metals, i.e. mixture M4

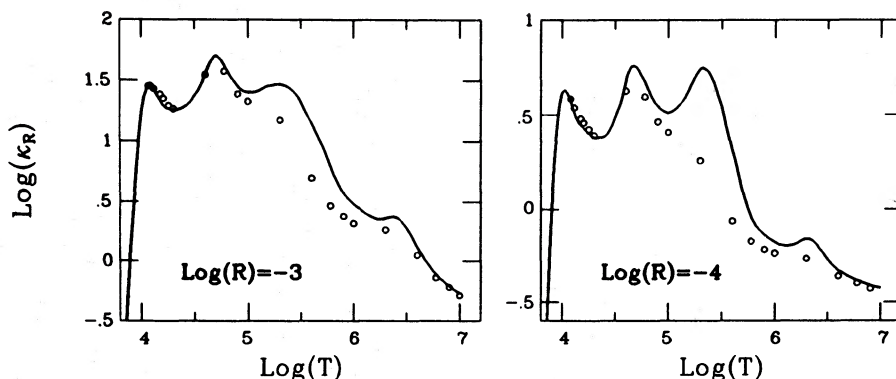


Figure 13. Rosseland mean opacities for $X=0.7$, $Z=0.02$, and Cox-Tabor abundances. Open circles represent results from LAOL, full lines those from OP.

of Weiss et al. The differences between the LAOL and OP results are largest in the region of the Z-bump and increase with decreasing density. For $\log(R) = -4$ and $\log(T) \approx 5.3$ the Rosseland means differ by a factor of about 3.

Magee, Merts & Hübner (1984), in defence of the LAOL opacities, argued that the enhancements postulated by Simon (1982) were incompatible with atomic physics. The deficiencies in the LAOL work have been discussed in several of the OPAL papers (see Rogers & Iglesias 1992). The most serious deficiencies concern the treatments of the spectral lines: in particular, the almost complete neglect of term-splitting and the neglect of transitions with $\Delta n = 0$. Magee et al. put some emphasis on the fact that, in the LAOL work, f -sum rules are correctly conserved, and this is discussed further by Sampson (1985). For the calculation of Rosseland means, however, a crucial question concerns the distribution of oscillator strength with frequency. The results obtained if one includes just one strong line for all transitions between two configurations are very different from the results obtained if one allows for all multiplet structures. We have seen that further changes can occur if the multiplets themselves are split into fine-structure components.

7.2 Comparisons with OPAL

7.2.1 Equations of State

Although the formulations of the EOS problem used by OPAL and OP appear to be very different, comparisons made by Däppen, Lebreton & Rogers (1990b), Däppen, Keady & Rogers (1990a) and Däppen (1991) show a generally close agreement between the OPAL and OP results for thermodynamic properties. For a few selected cases, comparisons of ionization equilibria have been made and good agreement obtained. Hummer (1988b) raises some questions concerning populations of high states which, according to the OP work, are highly dissolved.

7.2.2 Hydrogen and helium

In Figs 3 and 6, for hydrogen and helium, we include the OPAL results, shown as filled circles. Fig. 3 shows close agreement for hydrogen. In the region of the first maximum, $\log(T) \approx 4$, there is some sensitivity to the treatment of the far wings of the Lyman lines. In this region the largest

differences are seen for $\log(R) = -1$, where the OPAL results are about 10 per cent higher than those from OP. At higher densities there are differences of up to 13 per cent, with the OPAL results being the smaller. These differences occur in regions beyond, or close to, our boundary for envelopes [$\log(\rho) = -2$] and are almost certainly due to screening effects included in OPAL but neglected in OP. For hydrogen there is good agreement at the lowest temperatures considered (OPAL goes down to $T = 6000$, $\log(T) = 3.778$).

Fig. 6 shows that the agreement for helium is also generally close. There are some differences in the region of the first maximum, with the OPAL results being smaller than those of OP by up to 20 per cent at $\log(R) = -1$. Those differences are probably within the uncertainties in the theories used for treating the wings of the He I resonance lines. There are some significant differences at the lowest temperatures considered. Fig. 14 compares results for $\log(R) = -1$; similar discrepancies occur for other values of $\log(R)$.

7.2.3 Solar mix – without Cr, Mn and Ni

To compare like with like, we consider the 14-element G91 mix from OPAL (table 1 of Iglesias et al. 1992), omitting Cr, Mn and Ni. Small adjustments are made in the abundances of Ca and Fe in order to compensate partially for these omissions. We include fine structure for iron in both the OP and the OPAL data (the latter from Iglesias et al. 1992). Fig. 15 gives comparisons for $X=0.7$, $Z=0.02$. The overall agreement between OP and OPAL is seen to be satisfactory.

For the smaller values of $\log(R)$, OP gives a Z-bump in the vicinity of $\log(T) \approx 5.3$ which is slightly lower than that given by OPAL and is shifted to slightly higher temperatures.

At temperatures in the range $\log(T) = 4.0$ – 4.5 , the OPAL opacities are larger than those from OP; in this region OPAL has larger enhancements from the inclusion of iron fine structure. The results are in good agreement for $\log(T) \leq 4.0$ (the differences found in results for helium – see Fig. 14 – are of little importance for the mixture opacities). Fig. 16 shows low-temperature results for $\log(R) = -2$.

There are just two regions in which the OPAL opacities are 30 per cent larger than the OP ones. The first is at high densities, close to or beyond the boundary of the regions that we define as envelopes. Taking the limiting density to be

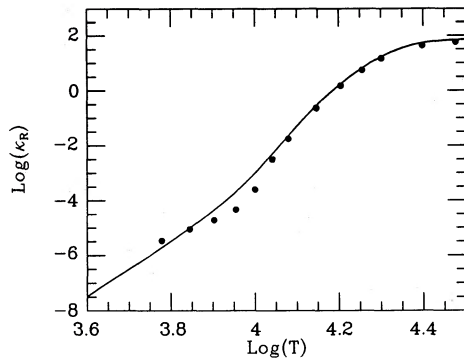


Figure 14. Rosselland mean opacities for helium at low temperatures. The case of $\log(R) = -1$ is shown. OP results are represented by the full line, OPAL results by the filled circles.

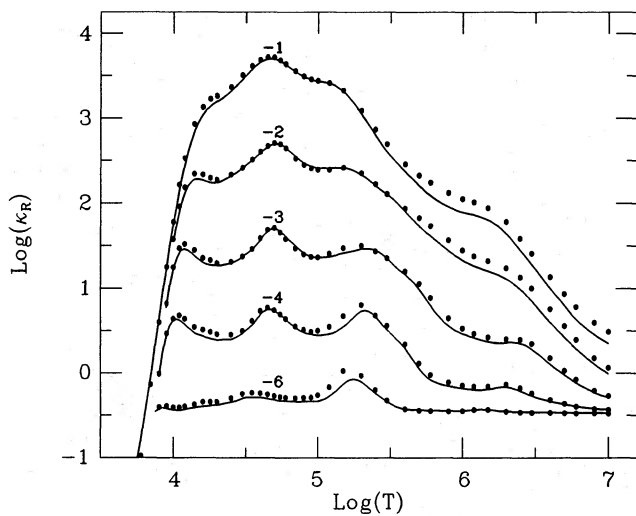


Figure 15. Opacities for $X=0.7$, $Z=0.02$, and the 14-element G91 mix (omitting Cr, Mn and Ni). OP results are represented by full lines, OPAL results by filled circles. Plots for five values of $\log(R)$ are shown.

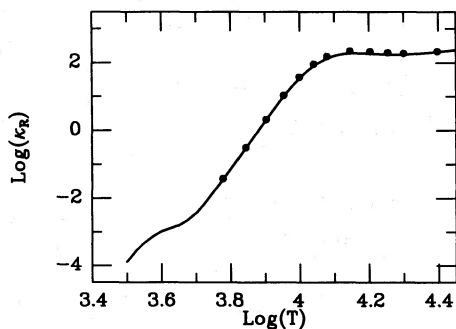


Figure 16. Low-temperature opacities for $\log(R) = -2$ are shown, for the same mixture as in Fig. 15. OP results are represented by full lines, OPAL results by filled circles.

$\log(\rho) = -2$, we obtain $\log(R) = 16 - 3 \log(T)$ for the boundary: hence $\log(T) = 5.667$ for $\log(R) = -1$ and $\log(T) = 6.0$ for $\log(R) = -2$. Near to and beyond this boundary, it is seen from Fig. 15 that there are differences

between the OP and OPAL results, with those of OPAL being the larger. We have investigated in some detail the case of $\log(T) = 6.0$ for which, of course, we have $\log(R) = \log(\rho)$. If we take the condition for the validity of the OP approach to be that there should be no significant dissolution of initial states contributing significantly to the opacity, then we find the condition to be satisfied at $\log(\rho) = -2$ but not satisfied at $\log(\rho) = -1$.

At $\log(T) = 6$, $\log(\rho) = -2$ the OPAL results are larger than those from OP by about 20 per cent. For this case we have performed some experiments in which we decrease the amounts of dissolution. We find that this leads to changes in the ionization equilibrium which lead to *decreases* in the Rosselland means, and hence to increased discrepancies with OPAL. The opacity results in this region are certainly sensitive to details of the EOS, and it is difficult to say whether the OP or OPAL results are to be preferred. Another point we note for this case is that there are important contributions from lines of the type $1s \rightarrow 2p$ and $1s^2 \rightarrow 1s2p$ in ions of C, N and O, and that the opacities are sensitive to the profile parameters used for these lines.

The case of $\log(T) = 6$, $\log(\rho) = -1$ definitely takes us beyond the range of validity of the approximations used in the OP work. For this case, the OPAL results are larger than the OP ones by about 30 per cent.

The other region with differences of about 30 per cent is at low densities and $\log(T) = 5.2$, as shown for the case of $\log(R) = -6$ in Fig. 15. In this region, as has already been noted by Rogers & Iglesias (1992), the calculations are very sensitive to details of the atomic physics used and of the elements included. For the case of $\log(T) = 5.2$ and $\log(R) = -6$ we have made the experiment of increasing the width parameters γ for all iron lines by a factor of 2, and find that this gives increases of about 30 per cent in the solar-mix opacities (see Section 6.4.6).

A further point concerning opacities at low densities must be borne in mind. The Rosselland mean opacities are small and the monochromatic opacities, at frequencies between spectral lines, may be even smaller. The Rosselland mean opacity is meaningful only when the diffusion approximation is valid at all frequencies, which requires that all monochromatic optical depths should be large.

7.2.4 Solar mix – inclusion of Cr and Ni

OPAL calculations have been made including Cr and Ni for $\log(R) = -5$ and for 10 temperatures in the range $(1.0-8.0) \times 10^5$ (see Rogers & Iglesias 1993). Fig. 17 gives a comparison between the OPAL and OP calculations for the ratios of Rosselland means with and without these other two elements. The magnitude of the enhancement is similar in both calculations.

7.2.5 Solar mix – the final results

Comparisons of like with like are obviously the most revealing in discussing the performances of the two sets of codes. On the other hand, the astronomer using the new opacities may be more interested in comparing the best results currently available. To meet this need we give, in Fig. 18, a comparison of the final OP results, including all four iron-group elements, and the OPAL results in which Cr, Mn

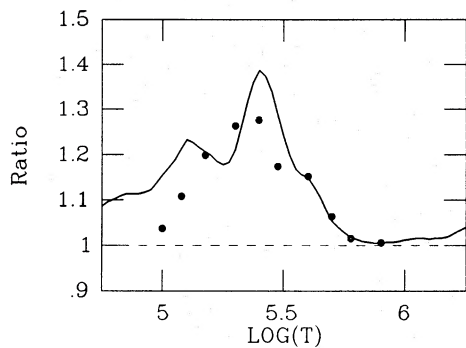


Figure 17. The ratio of Rosseland means with and without inclusion of the elements Cr and Ni, for $\log(R) = -5$. OP results are represented by the full line, OPAL results by the filled circles.

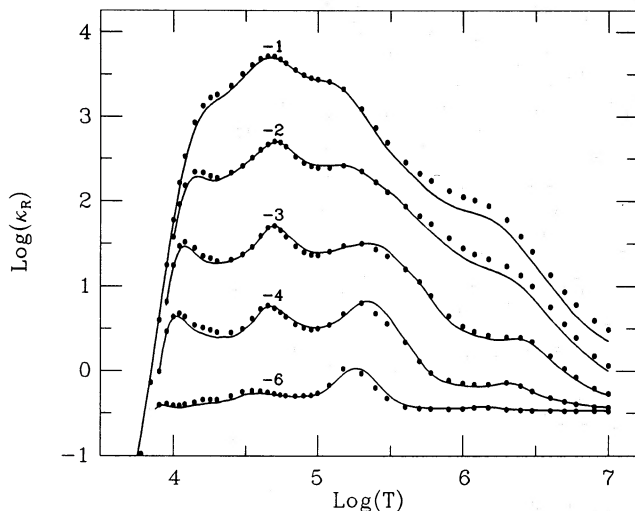


Figure 18. Comparison of OP opacities using S92 abundances (full lines) and OPAL opacities using G91 abundances (filled circles), for $X = 0.70$, $Z = 0.02$. The only significant difference between the two sets of abundances is the omission of Cr, Mn and Ni in G91.

and Ni are omitted. The improvement in the agreement between OP and OPAL shown in Fig. 18, compared with that of Fig. 15, must be regarded as largely fortuitous.

Quite extensive new pulsation calculations have already been made using the new opacities, mainly those from OPAL but also with some use of those from OP (Cox 1991; Kovacs, Buchler & Marom 1991; Cox et al. 1992; Kiriakidis, El Eid & Glatzel 1992; Moskalik, Buchler & Marom 1992; Moskalik & Dziembowski 1992; Stothers 1992; Stothers & Chin 1992; Dziembowski & Pamyatnykh 1993; Gautschy & Saio 1993; Glatzel, Kiriakidis & Fricke 1993; Glatzel & Kiriakidis 1993). Those calculations show that use of the new opacities resolves a number of outstanding problems in the theories of pulsating stars. Further calculations using both OP and OPAL opacities, as considered in Fig. 18, have been made by Kanbur & Simon (1994) for beat and bump Cepheids. They find that these two sets of opacities give pulsation results that are almost exactly the same.

7.2.6 A metal-rich case

For Fig. 19 we use the same relative abundances of metals as those used for Fig. 18, but now consider the metal-rich case of $X = 0.70$, $Z = 0.04$.

7.3 Summary of comparisons of OP and OPAL

The following points are worth noting.

(1) In envelope regions there are probably no important differences between the results for opacities due to different treatments of EOS problems.

(2) The OP atomic data are more accurate than the OPAL atomic data. There is, however, no reason to suspect systematic errors in the OPAL data; higher accuracy for individual transitions may not be important when very large numbers of transitions are involved. The comparison of the results from the two projects shows, as far as the accuracy of atomic data is concerned, that convergence has almost certainly been obtained. In addition to the accuracy of atomic data, it is also important to consider the completeness of the data included. This has been checked in the work of both projects.

(3) OP allows for auto-ionization broadening, neglected by OPAL, but neglects pressure broadening of auto-ionization features which may be important at higher densities.

(4) In both projects calculations have been made including fine structure for iron. OPAL includes intercombination lines neglected by OP. On the other hand, OP includes 'two-electron jumps' neglected by OPAL.

(5) The elements Cr, Mn and Ni are included in the OP work for all temperatures and densities. OPAL has included these three elements only for a few check points.

We have not kept an exact count of the amount of super-computer time used in the OP work. It must certainly be measured in thousands of hours. We expect that a comparable amount has been used in the OPAL work. The two projects are entirely independent and it is very gratifying, at the end of the day, that there are no serious discrepancies in the results obtained.

8 CONCLUSION

Extensive atomic data have been obtained in the course of the OP work and are being made generally available. On request, we can provide OP Rosseland mean opacities for envelopes, for any required chemical mixture.

The new opacities from OP and OPAL are in substantial agreement. For certain regions of temperature and density there are large differences between the new opacities and the older opacities from LAOL. The new opacities have been used in a wide range of problems: theories of stellar pulsation; excitation of pulsation in β Cephei stars; the dependence of pulsation on metallicity; the mass limit for pulsational stability; post-main-sequence evolution; and the solar radiative interior (a problem outside the range of the OP work).

In all cases, use of the new opacities gives improved agreement between observations and astrophysical theory. We conclude that both of Eddington's clouds have now been dispersed.

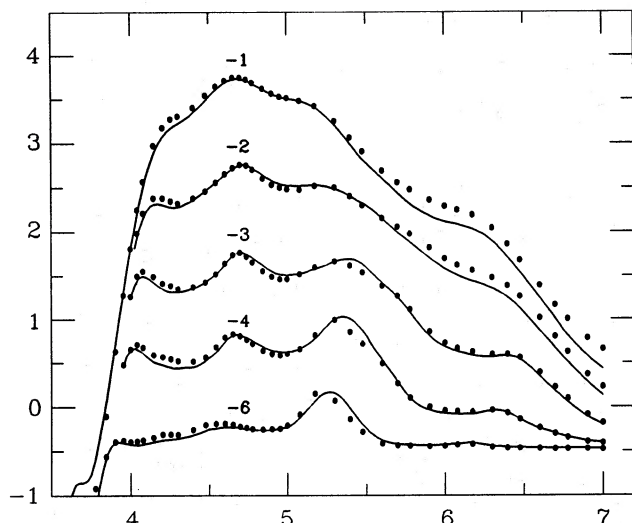


Figure 19. As Fig. 18, using the same relative abundances of metals but with $X=0.70$, $Z=0.04$.

ACKNOWLEDGMENTS

The Opacity Project was first conceived in discussions between David Hummer, DM and MJS in 1983 May. David Hummer first suggested the need to make level-by-level atomic data calculations, and provided invaluable comments on all later aspects of the work.

The project has depended essentially on the work of a large team which has cheerfully carried out the atomic physics work. We give our heartfelt thanks to all team members. Special mention must be made of the group at The Queen's University of Belfast, led by Professor P. G. Burke, for supplying the basic R -matrix codes and contributing to both code development and atomic data production.

We thank Achim Weiss for providing the data on stellar models used in plotting Figs 1 and 2, and for advice on the opacity requirements for work on stellar structure.

We extend special thanks to Carlos Iglesias and Forrest Rogers for much-valued comments and advice, and for their generous hospitality during a visit by YY and MJS to their laboratory in 1991 December.

AKP acknowledges partial support from the US National Science Foundation through grants AST-8996215, PHY-91150597 and INT-9013946.

MJS acknowledges support from the Science and Engineering Research Council (SERC) through the award of a 4-year Senior Research Fellowship and several research grants. Work on the IBM-3090 at the Rutherford and Appleton Laboratory (RAL) was supported by the IBM-SERC Joint Study Initiative and by other SERC grants. MJS thanks RAL computer staff for their help in the use of CRAY, IBM and DEC machines.

DM acknowledges support through grant numbers AST 85-19209 and AST 89-14143 from the National Science Foundation. We especially thank the National Center for Supercomputer Applications (University of Illinois) for several generous allocations of computer time, which made successful completion of this project possible.

Support is also acknowledged through a grant from the NASA Astrophysical Theory Program to the University of

Colorado, and two NATO travel grants to University College London.

REFERENCES

- References to papers in the series 'Equations of State for Stellar Envelopes' are given in Table 1, and those to papers in the series 'Atomic Data for Opacity Calculations' in Table 1.
- Allard N., Artru M.-C., Lanz T., Le Dourneuf T., 1990, *A&AS*, 84, 563
- Anders E., Grevesse N., 1989, *Geochim. Cosmochim. Acta*, 53, 197
- Andreasen G. K., 1989, in Schmidt E. G., ed., *IAU Colloq. No. 111, Use of Pulsating Stars in Fundamental Problems of Astronomy*. Cambridge Univ. Press, Cambridge, p. 248
- Becker S. A., 1985, in Madore B. F., ed., *Cepheids: Theory and Observation*. Cambridge Univ. Press, Cambridge, p. 104
- Bell K. L., Berrington K. A. B., 1987, *J. Phys. B*, 20, 801
- Bell K. L., Berrington K. A. B., Croskey P. J., 1982, *J. Phys. B*, 15, 977
- Boercker D. B., 1987, *ApJ*, 316, L98
- Carson T. R., 1976, *ARA&A*, 14, 95
- Carson T. R., Mayers D. F., Stibbs D. W. N., 1968, *MNRAS*, 140, 483
- Cox A. N., 1965, in Aller L. H., MacLaughlin D. B., eds, *Stellar Structure*. Univ. Chicago Press, Chicago, p. 195
- Cox A. N., 1991, *ApJ*, 381, L71
- Cox A. N., Stewart J. N., 1962, *ApJ*, 67, 113
- Cox A. N., Morgan S. M., Rogers F. J., Iglesias C. A., 1992, *ApJ*, 392, 272
- Cunto W., Mendoza C., 1992, *Rev. Mex. Astron. Astrofis.*, 23, 107
- Cunto W., Mendoza C., Ochsenbein F., Zeippen C. J., 1993, *A&A*, 275, L5
- Däppen W., 1991, *Rev. Mex. Astron. Astrofis.*, 23, 141
- Däppen W., Anderson L. S., Mihalas D., 1987, *ApJ*, 319, 195
- Däppen W., Keady J., Rogers F. J., 1990a, in Cox A. N., Livingston W. C., Mathews M., eds, *Solar Interior and Atmosphere*, Space Science Series. Univ. Arizona Press, Arizona
- Däppen W., Lebreton Y., Rogers F., 1990b, *Solar Phys.*, 128, 35
- Dziembowski W. A., Pamyatnykh A. A., 1993, *MNRAS*, 262, 204
- Eddington A. S., 1926, *The Internal Constitution of the Stars*. Cambridge Univ. Press, Cambridge
- Eiassner W., Nussbaumer H., 1969, *J. Phys. B*, 2, 1028
- Fricke K., Stobie R. S., Strittmatter P. A., 1971, *MNRAS*, 154, 23
- Gautschy A., Saio H., 1993, *MNRAS*, 262, 213
- Glatzel W., Kiriakidis M., 1993, *MNRAS*, 262, 85
- Glatzel W., Kiriakidis M., Fricke K. J., 1993, *MNRAS*, 262, L7
- Graboske H. C., Harwood D. J., Rogers F. J., 1969, *Phys. Rev.*, 186, 210
- Grevesse N., Noels A., 1993, in Prantzo N., Vangioni-Flam E., Casse M., eds, *Origin and Evolution of the Elements*. Cambridge Univ. Press, Cambridge
- Grevesse N., Noels A., Sauval A. J., 1992, in Domingo V., ed., *Coronal Streamers, Coronal Loops and Coronal and Solar Wind Composition*. ESA Publications Division, Noordwijk
- Griem H. R., 1974, *Spectral Line Broadening by Plasmas*. Academic Press, New York
- Hibbert A., 1975, *Comput. Phys. Commun.*, 9, 141
- Hübner W. F., 1985, in Sturrock P., Holzer T., Mihalas D., eds, *Physics of the Sun*. Reidel, Dordrecht, p. 33
- Hübner W. F., Merts A. L., Magee N. H., Argo M. F., 1977, *Los Alamos Report LA-6760-M*
- Hummer D. G., 1988a, *ApJ*, 327, 477
- Hummer D. G., 1988b, in Hauer A., Merts A. L., eds, *Proc. Conf. Atomic Physics in Plasmas*. American Institute of Physics, New York, p. 1

- Iglesias C. A., Rogers F. J., 1991a, ApJ, 371, 408
 Iglesias C. A., Rogers F. J., 1991b, ApJ, 371, L73
 Iglesias C. A., Rogers F. J., Wilson B. G., 1987, ApJ, 322, L45
 Iglesias C. A., Rogers F. J., Wilson B. G., 1990, ApJ, 360, 221
 Iglesias C. A., Rogers F. J., Wilson B. G., 1992, ApJ, 397, 717
 Kanbur S., Simon N., 1994, ApJ, in press
 Kiriakidis M., El Eid M. F., Glatzel W., 1992, MNRAS, 255, 1P
 Kovacs G., Buchler J. R., Marom A., 1991, A&A, 252, 127
 Le Dourneuf M., Nahar S. N., Pradhan A. K., 1993, J. Phys. B, 26, L1
 Magee N. H., Merts A. L., Hübner W. F., 1984, ApJ, 283, 264
 Mayer H., 1947, Los Alamos Report LA-647
 Meyerott R. E., Moszkowski S. A., 1951, Rep. ANL-4594, Argonne National Lab.
 Mihalas D., 1978, Stellar Atmospheres, 2nd edn. Freeman, San Francisco
 Moore C. E., 1970, National Bureau of Standards, Report NSRDS-NBS 34
 Moskalik P., Dziembowski W. A., 1992, A&A, 256, L5
 Moskalik P., Buchler J. R., Marom A., 1992, ApJ, 385, 685
 Moszkowski S. A., Meyerott R. E., 1951, Rep. ANL-4743, Argonne National Lab.
 Nussbaumer H., Storey P. J., 1978, A&A, 64, 139
 Petersen J. O., 1974, A&A, 34, 309
 Rogers F. J., Iglesias C. A., 1993, in Nemeč J. M., Mathews J. M., eds, IAU Colloq. No. 139, New Perspectives on Stellar Pulsations and Pulsating Variable Stars. Cambridge Univ. Press, Cambridge, p. 221
 Rogers F. J., Iglesias C. A., 1992, ApJS, 79, 507
 Sampson D. H., 1985, J. Quantit. Spectrosc. Radiat. Transfer, 34, 347
 Schwarzschild M., 1958, Structure and Evolution of the Stars. Princeton Univ. Press, Princeton
 Seaton M. J., 1983, Rep. Prog. Phys., 46, 167
 Seaton M. J., 1993, MNRAS, 265, 25P
 Simon N. R., 1982, ApJ, 260, L87
 Stellingwerf R. F., 1978, AJ, 83, 1184
 Storey P. J., Hummer D. G., 1991, Comput. Phys. Commun., 66, 129
 Stothers R. B., 1992, ApJ, 392, 706
 Stothers R. B., Chin C.-w., 1992, ApJ, 390, 136
 Weise W. L., Kelleher D. E., Paquette D. R., 1972, Phys. Rev. A, 6, 1132
 Wiese W. L., Deters T. M., Fuhr J. R., 1994, J. Phys. Chem. Ref. Data, Monograph Series, in press
 Weiss A., Keady J. J., Magee N. H., 1990, Atomic Data Nucl. Data Tables, 45, 209
 Wishart A., 1979, MNRAS, 53, 59P

APPENDIX A: DISSOLVED LINES, RAYLEIGH SCATTERING AND FAR LINE-WINGS

We discuss some further technical details concerning dissolved lines, Rayleigh scattering and far line-wings.

A1 Contributions to opacities from dissolved lines

As levels dissolve one obtains highly perturbed states, effectively spread out to give a continuum. In consequence the lines in each spectral series become increasingly broad and eventually merge into a continuum which is a below-threshold extrapolation of that due to photoionization. A similar effect can, of course, be described in terms of the lowering of the ionization potential of the initial state, but such a treatment may not show the transition from broad blended lines to a continuum.

In this appendix we use atomic units, a_0^2 , for cross-sections and Rydberg units for energies [$E(\text{Ry}) = 2 \times E(\text{atomic units})$]. The cross-section for absorption in a spectral line with initial level i and final level f , both assumed to be undissolved, is

$$\sigma_i^{(\text{line})}(\omega) = 4\pi^2 \alpha f(f, i) \phi(\omega) \quad (\text{undissolved}), \quad (\text{A1})$$

where ω is the photon energy, $f(f, i)$ the oscillator strength, $\phi(\omega)$ the line profile and α the fine-structure constant ($\alpha \approx 1/137$).

The cross-section for photoionization from level i is

$$\sigma_i^{(\text{PI})}(\omega) = 4\pi^2 \alpha \frac{df(\omega, i)}{d\omega}, \quad (\text{A2})$$

where $df(\omega, i)/d\omega$ is the differential oscillator strength.

Consider absorption in a spectral series in which an upper level has an effective quantum number $\nu = n - \mu$, where μ is a quantum defect. The energy of the upper level, relative to the ionization limit, is $E = -Z^2/\nu^2$, where Z is the charge on the ion core. Assuming μ to be approximately constant, the separations between high adjacent levels (n differing by unity) is $\Delta E = 2Z^2/\nu^3$. A mean photoabsorption cross-section is defined by

$$\sigma_i^{(\text{PA})}(\omega_i) = 4\pi^2 \alpha \times \frac{f(f, i)}{\Delta E}. \quad (\text{A3})$$

It may be shown (see, for example, Seaton 1983) that $\sigma_i^{(\text{PA})}(\omega)$ is the analytic continuation of $\sigma_i^{(\text{PI})}(\omega)$. We assume that fully dissolved lines give cross-sections $\sigma_i^{(\text{PA})}(\omega)$. Let ω_i be the threshold for true photoionization. Our calculations are extended down to

$$\omega = \omega_i - Z^2/\nu_0^2, \quad (\text{A4})$$

with $\nu_0 = 10$, giving cross-sections $\sigma_i^{(\text{PA})}(\omega)$. We include spectral lines only for states in which the final state has an effective quantum number $\nu_f \leq \nu_0$. All levels with $\nu_f > \nu_0$ are assumed to be fully dissolved and to give absorption cross-sections $\sigma_i^{(\text{PA})}(\omega)$.

A1.1 Non-hydrogenic systems

For non-hydrogenic systems we use Lorentz line profiles

$$\phi(\gamma, x) = (\gamma/\pi) \{x^2 + \gamma^2\}^{-1}, \quad (\text{A5})$$

where $x = |\omega - \omega_{fi}|$. These profiles are, of course, always convolved with those for thermal Doppler broadening. Consider an upper state f that is partially dissolved. There is a probability $W(f)$ that the state exists. Däppen, Anderson & Mihalas (1987) argue that, if an atom is in an environment such that the upper level exists, then the lower level certainly exists. They therefore take the cross-section, for a partially dissolved upper state, to be

$$\sigma_{fi}^{(\text{line})}(\omega) = 4\pi^2 \alpha f(f, i) \phi(\omega) \times \frac{W(f)}{W(i)} \quad (\text{partially dissolved}), \quad (\text{A6})$$

¹Strictly speaking, we take $\nu_0 = 10$ only when the initial state has an effective quantum number $\nu_i < 5$; if $\nu_i > 5$ we take $\nu_0 = 2\nu_i$.

where we recalled that the cross-section is to be multiplied by N_i calculated with inclusion of the factor $W(i)$ in (19). Däppen et al. take the contribution from dissolved lines to be

$$\sigma_i^{(\text{DL})}(\omega) = \sigma_i^{(\text{PA})}(\omega) \times \left[1 - \frac{W(f)}{W(i)} \right], \quad (\text{A7})$$

where f is here taken to be a continuous variable corresponding to the effective quantum number ν_r .

In practice it is difficult to use (A7) for complex systems, for which configuration-interaction effects can cause $\sigma_i^{(\text{PA})}(\omega)$ to have a complicated dependence on ω . For the dissolved-line contributions we use Lorentz profiles with widths $\delta = (1/2)\Delta E = Z^2/\nu_j^3$. The total contribution from a given upper level is then taken to be that obtained from (A1) with

$$\phi(\omega) = \phi(\gamma, x) \times [W(f)/W(i)] + \phi(\delta, x) \times [1 - W(f)/W(i)]. \quad (\text{A8})$$

This gives results similar to those that would be obtained using (A6) and (A7), but with a slightly ‘wiggly’ appearance.

A1.2 Hydrogenic systems

For transitions $n \rightarrow n'$ in a hydrogenic ion of nuclear charge Z , we use the theory discussed in ADOC XIII. We have already taken account of dissolution in calculating the line profiles with normalization (45), and equation (A6) is therefore used omitting the factor $W(f)$. The cross-sections $\sigma_i^{(\text{PA})}(\omega)$ are easily calculated, and equation (A7) is used. The theory gives good agreement with experimental results from Wiese, Kelleher & Paquette (1972) for the region of high blended Balmer lines.

A1.3 He I resonance lines

For the cores of He I resonance lines ($1s^2\ ^1S \rightarrow 1snp\ ^1P^0$) we use Lorentz profiles with values of γ taken from Griem (1974). For the wings we use whichever is the larger, the Lorentz profile or a modified hydrogenic profile. We use accurate values, for He I, of $\sigma_i^{(\text{PI})}(\omega)$ and $\sigma_i^{(\text{PA})}(\omega)$.

A2 Rayleigh scattering

Rayleigh scattering can be important at low temperatures, at which all atoms are mostly neutral. We include it only for neutral H and He, assuming that these two atoms will always be the most abundant.

Consider first a classical model of an electron attached to a simple harmonic oscillator with frequency ω_0 . The Rayleigh cross-section is

$$\sigma_R(\omega) = \sigma_T \omega^4 |I(\omega)|^2, \quad (\text{A9})$$

where $\sigma_T = 8\pi\alpha^4/3$ is the Thomson cross-section,

$$I(\omega) = \frac{1}{\omega_0^2 - \omega^2 + 2i\gamma_c\omega} \quad (\text{A10})$$

and $\gamma_c = \alpha^3\omega_0^2/6$ is the classical damping constant. We take the quantum-mechanical generalization of (A10) to be

$$I(\omega) = \sum_{n \geq 2} \frac{f_n}{\omega_n^2 - \omega^2 + 2i\gamma_n\omega}, \quad (\text{A11})$$

where $n=2$ is the first excited state having an optically allowed transition to the ground state, ω_n is the photon energy for the $1 \rightarrow n$ transition, $f_n = f(n, 1)$ is the oscillator strength for that transition, and $\gamma_n = f_n \times \gamma_c$. This gives the following limiting cases:

(i) the Kramers–Heisenberg dispersion formula

$$I(\omega) = \sum_{n \geq 2} \frac{f_n}{\omega_n^2 - \omega^2} \quad \text{for } (\omega_2 - \omega) \gg \gamma_2; \quad (\text{A12})$$

(ii) $I(0) = P/4$, where P is the dipole polarizability of the ground state;

(iii) for $\omega \approx \omega_n$, the usual expression for a line allowing for radiation damping in the $n \rightarrow 1$ transitions,

$$\sigma_R = 4\pi^2 \alpha f_n \phi(\gamma_n, \omega); \quad (\text{A13})$$

(iv) $\sigma_R(\omega) = \sigma_T$ in the limit of $\omega \rightarrow \infty$.

We are interested in energies ω up to and including the immediate vicinity of the first line. We put

$$I(\omega) = \frac{f_2}{\omega_2^2 - \omega^2 + 2i\gamma_2\omega} + K(\omega), \quad (\text{A14})$$

where

$$K(\omega) = \sum_{n \geq 3} \frac{f_n}{\omega_n^2 - \omega^2}. \quad (\text{A15})$$

A good approximation is given by

$$K(\omega) = \frac{\bar{f}}{\bar{\omega}^2 - \omega^2}. \quad (\text{A16})$$

The constants \bar{f} and $\bar{\omega}$ (which are adjusted to give accurate values of the polarizability P) are given in Table A1.

Using (A14) we obtain

$$|I(\omega)|^2 = \frac{\theta(\omega)f_2}{(\omega_2 + \omega)^2} [f_2 + 2(\omega_2^2 - \omega^2)K(\omega)] + K(\omega)^2, \quad (\text{A17})$$

where

$$\theta(\omega) = 1 / \{(\omega_2 - \omega)^2 + \gamma_2^2 [2\omega / (\omega_2 + \omega)]^2\}. \quad (\text{A18})$$

Table A1. Rayleigh-scattering parameters for H and He.

	H	He
P	4.5	1.38323
ω_2	0.75	1.5597
f_2	0.4162	0.2811
$\bar{\omega}$	1.016	1.968
\bar{f}	0.3975	0.8918

In (A18), the term in γ_2^2 is non-negligible only for small $|\omega_2 - \omega|$ and we may therefore put $[2\omega/(\omega_2 + \omega)]^2 = 1$ to obtain

$$\sigma(\omega) = 4\pi^2 \alpha Q(\omega) \phi(\gamma_2, \omega) [f_2 + 2(\omega_2^2 - \omega^2)K(\omega)] + \sigma_T \omega^4 K(\omega)^2, \quad (\text{A19})$$

where $\phi(\gamma_2, \omega)$ is given by (A5) and

$$Q(\omega) = \{2\omega^2 / [\omega_2(\omega + \omega_2)]\}^2. \quad (\text{A20})$$

Note that $Q(\omega) \approx 1$ for $\omega \approx \omega_2$ and that $Q(\omega) \approx 4(\omega/\omega_2)^4$ for $\omega \ll \omega_2$.

A3 Far line-wings

Far line-wings can make significant contributions to opacities. Far blue-wings are not usually of much importance because to the blue side of a spectral line one has contributions from other lines and, eventually, from photoionization. Far red-wings can pose problems and, to our knowledge, no completely satisfactory theory is yet available.

The problems encountered are most serious for temperatures and densities such that most atoms are neutral, since then one has only small background contributions from electron scattering and electron-ion free-free transitions.

For the case in which radiation damping is the only line-broadening mechanism, equations (A19) and (A20) provide convenient working formulae for the region up to and including the vicinity of the first resonance line. In practice it is usually necessary to include the effects of pressure broadening. The usual pressure-broadening theories give profiles with wings behaving like $|\omega_n - \omega|^{-\beta}$, with $\beta = 2$ or $5/2$. Such wing formulae are not valid when $|\omega_n - \omega|$ is large; they give finite values for profiles in the limit of $\omega \rightarrow 0$, which are certainly incorrect. In some cases we find that the use of such profiles can lead to large errors in the calculated single-element opacities.

It follows from (A19) and (A20) that cross-sections calculated allowing for radiation damping tend to zero in the limit of $\omega \rightarrow 0$, behaving like ω^4 . A similar behaviour is expected when pressure broadening is included. Since we lack a satisfactory theory for the far wings of the pressure-broadened lines, we make use of formulae based on (A19) and (A20) for the red wings of the lines.

A3.1 Hydrogen lines

The problem of how to handle far wings in hydrogenic systems arises only for the Lyman lines. Consider first the lines $1 \rightarrow n$ with $n \geq 3$. In the line-broadening theory used (see ADOC XIII) we exclude all microfield broadening that gives shifts larger than one-half of the distance to the next line, $(\omega_n - \omega) > (\omega_n - \omega_{n-1})/2$. We do include some contribution from electron broadening beyond that point, but the theory certainly breaks down if continued much beyond it. Our procedure for all lines with $n \geq 3$ is to neglect all pressure broadening that gives shifts larger than the distance to the next lower line, $(\omega_n - \omega) > (\omega_n - \omega_{n-1})$. In using (A19) we do, however, include allowance for the radiation-damping far wings.

For the region of $\omega \leq \omega_2$ we use (A19) with a profile $\phi_2(\omega)$ calculated allowing for radiation damping and for pressure broadening.

A3.2 Helium lines

For the higher resonance lines we use Lorentz profiles (convoluted with Doppler broadening to give Voigt profiles) with parameters γ being the sums of contributions from electron-impact broadening and radiation damping. The profiles are stopped at shifts corresponding to the next lower line. For the first resonance line, $n=2$, we use a modified hydrogenic red wing (allowing for microfield broadening) and, for $\omega \leq \omega_2$, we use equation (A19).

A3.3 Other resonance lines

Our calculations are extended down to temperatures of $\log(T) = 3.5$. At the lower temperatures considered we encounter special problems concerning far line-wings. Neutral atoms provide the dominant ionization stage. For elements other than H and He we do not include electron-neutral free-free transitions and Rayleigh scattering. The main contributions to opacities for these elements, at low temperatures and at frequencies of importance for the calculation of Rosseland means, are then due to photoionization from excited states (in order to obtain convergence it is necessary to include high excited states with fractional populations as low as 10^{-10} or even smaller). In such circumstances the monochromatic opacities are small and we find that very far red-wings of resonance lines, calculated using Lorentz profiles, can make important contributions. Such contributions are almost certainly spurious and, since we lack a satisfactory theory for the far-wing profiles, we adopt the expedient of multiplying the red-wing profiles by factors of $(\omega/\omega_{mn})^4$:

$$\phi(\omega) = (\omega/\omega_{mn})^4 \times \phi(\gamma, |\omega - \omega_n|) \quad (\text{for } \omega < \omega_n). \quad (\text{A21})$$

An illustrative result is shown in Fig. A1, which gives the cross-section σ for Na at $\log(T) = 4.5$, $\log(N_e) = 17.5$ [corre-

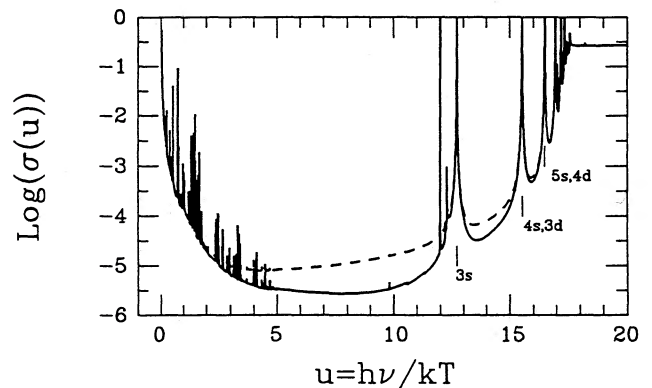


Figure A1. The opacity cross-section σ for Na, $\log(T) = 4.5$, $\log(N_e) = 17.5$. For these conditions, 98 per cent of the Na is in the Ne-like stage, Na II. The plot shows the effects of far line-wings. The dashed line shows the result without the factor $(\omega/\omega_{mn})^4$ in equation (A21), and the full line the result with that factor.

sponding, for a solar mix, to $\log(\rho) = -6.16$, $\log(R) = -1.66$]. For this case, 98 per cent of the Na is in the ionization stage Na II and, using Lorentz profiles, there are large contributions to the Rosseland mean from far wings of the lines Na II $2p^6 \rightarrow 2p^5ns$, nd. The dashed line in Fig. A1 is calculated using unmodified Lorentz profiles, and the full

line with inclusion of the factor $(\omega/\omega_n)^4$ in (A21), which is seen to result in a marked decrease in the contributions from the line wings. The Rosseland means are 10.57×10^{-6} and 4.53×10^{-6} for the two cases, in units of a_0^2 . Use of the factors $(\omega/\omega_n)^4$ as in (A21) or $Q_n(\omega) = \{2\omega^2/[\omega_n(\omega + \omega_n)]\}^2$ as in (A20) gives nearly the same result.